New estimation of NO x snow-source on the Antarctic Plateau for a better global model parameterization

Albane Barbero, J. Savarino, C. Blouzon, M. Frey, G. Picard, S Ahmed, C Amory, J Thomas, Y. Huang, N. Caillon, et al.

▶ **To cite this version:**

Albane Barbero, J. Savarino, C. Blouzon, M. Frey, G. Picard, et al.. New estimation of NO x snow-source on the Antarctic Plateau for a better global model parameterization. Journal of Geophysical Research: Atmospheres, 2021, 126 (20), 10.1029/2021JD035062 . hal-03402244

HAL Id: hal-03402244
https://hal.science/hal-03402244

Submitted on 25 Oct 2021

HAL is a multi-disciplinary open access archive for the deposit and dissemination of scientific research documents, whether they are published or not. The documents may come from teaching and research institutions in France or abroad, or from public or private research centers.

L'archive ouverte pluridisciplinaire **HAL**, est destinée au dépôt et à la diffusion de documents scientifiques de niveau recherche, publiés ou non, émanant des établissements d'enseignement et de recherche français ou étrangers, des laboratoires publics ou privés.

New estimation of NO_x snow-source on the Antarctic Plateau for a better global model parameterization

A. Barbero[1], J. Savarino[1], C. Blouzon[1], M. Frey[2], G. Picard[1], S. Ahmed[1], C. Amory[1], J. Thomas[1], Y Huang[3], N. Caillon[1], and R. Grilli[1]

[1]*Univ. Grenoble Alpes, CNRS, IRD, Grenoble INP (Institute of Engineering), IGE, Grenoble, France*

[2]*British Antarctic Survey, Natural Environment research Council, Cambridge, CB3 0ET, UK*

[3]*Department of Civil and Environmental Engineering, Wayne State University, Detroit, MI, USA*

Corresponding author: Albane Barbero albane.barbero@univ-grenoble-alpes.fr

Key points

Antarctic Plateau; Oxidative capacity; Snowpack emissions; Flux chamber; Nitrate photolysis; Model parameterization

Abstract

To fully decipher the role of nitrate photolysis on the oxidative capacity in snow-covered regions, improvements to the uncertainties of NO_x flux estimates and global atmospheric models are strongly needed. Here, we introduce a method based on dynamic flux chamber measurements for evaluating the NO_x flux emitted by photolysis of snowpack nitrate in Antarctica. For the first time in the field, flux chamber experiments were conducted at the French-Italian station Concordia, Dome C (75°06'S, 123°20'E, 3233m a.s.l) during the 2019-2020 summer campaign. Tests were performed with several snows of different ages ranging from newly formed drift snow to 16-20-year-old firn. Surprisingly, the same daily average photolysis rate constant, $\overline{J_{NO_3}}$, of (3.94 ± 0.68) x 10^{-8} s^{-1} (1σ) was obtained for the different types of snow samples, suggesting that the photolabile nitrate in snow behaves as a single-family source with common photochemical properties. Summer daily average NO_x fluxes, $\overline{F_{NO_x}}$, were estimated to be (7.9 ± 4.3) x 10^{7} molecules cm^{-2} s^{-1}, ~ 5 to 40 times less than what has been estimated in previous studies at Dome C and with uncertainties reduced by a factor up to 20. Using these results, we extrapolated an annual continental snow source NO_x budget of 0.045 ± 0.015 Tg.N y^{-1}, more than five times the N-budget of the stratospheric denitrification previously estimated for Antarctica. This innovative approach to the parameterization of nitrate photolysis using flux chamber experiment could likely reduce modeling uncertainties and serve as a guide for future model improvements.

1. Introduction

The southern high-latitude regions of Antarctica are ideal for studying the connections between climate and atmospheric chemistry due to distinct geographic advantages. Antarctica's great distance from major sources of pollution, the outflow of low-level katabatic winds, and the insulating nature of the atmospheric circulation combine to maintain a relative cleanliness *(Savitskiy and Lessing, 1979)*. Therefore, Antarctica is often considered to be the last continental-sized natural laboratory. Snow-air-radiation interactions and their link to the specific oxidizing character of the polar atmosphere is key to correctly decipher the past environmental information preserved in the ice and understand the present chemical stability of the glacial atmosphere. Previous studies presented observations suggesting the existence of a highly reactive lower atmosphere above the snowpack *(Domine and Shepson, 2002; Grannas et al., 2007)*. These puzzling findings raise questions about possible alterations of the background air composition within the polar atmosphere. Unexpectedly high levels of oxidants have been discovered in the continental interior as well as in the coastal regions, with atmospheric hydroxyl radical (OH) concentrations up to 4 x 10^6 cm^{-3} *(Davis et al., 2008; Grilli et al., 2013; Kukui et al., 2014; Mauldin et al., 2010, 2001, 2004; Wang et al., 2007)*. These levels make the summer Antarctic boundary layer as oxidative as urban atmospheres and well beyond what was expected for an atmosphere thought to have the most pristine boundary layer on Earth *(Bloss et al., 2005; Saiz-Lopez et al., 2017; Volkamer et al., 2010)*. It is now well established that such high reactivity of the summer Antarctic boundary layer results, in part, from the emissions of nitrogen oxides ($NO_x \equiv NO + NO_2$) produced during the photo-denitrification of the snowpack when subject to intense ultraviolet (UV) *(Honrath et al., 1999, 2000; Jones et al., 2000, 2001)*. Despite the numerous observations collected at various sites during previous campaigns such as ISCAT 1998, 2000, ANTCI and OPALE, *(Davis et al., 2008; Mauldin et al., 2001, 2004; Preunkert et al., 2012; Wang et al., 2007)*, a robust quantification of the NO_x sources on a continental scale over Antarctica is still lacking *(Frey et al., 2013a, 2015a; Legrand et al., 2014; Savarino et al., 2016)*. The chemical reactivity of the snowpack and its connection to the overlying oxidative atmosphere need further study to better understand their linkage to the snow chemical composition.

Previous works have proposed different mechanisms to explain the nitrate photolysis behavior in ice and snow *(Blaszczak-Boxe and Saiz-Lopez, 2018 and references therein)*. Chu and Anastasio (2003) studied the nitrate photolysis on ice and their results suggested that the ice nitrate photolysis is occurring in a "quasi-liquid layer" rather than in the bulk ice *(Chu and Anastasio, 2003)*. Davis et al. (2008), developed a theory driven by two photo-chemical domains affecting the nitrate photo-dissociation, namely the photo-labile and buried domains *(Davis et al., 2008)*. Zatko et al. (2013) followed Davis et al. (2008) by assuming that the NO_3^- incorporated in the snowpack by wet deposition is ingrained in the snow crystal compared to dry NO_3^- deposition, where it stays at the surface of the snow-grain, therefore more likely to dissociate into NO_x after encountering a photon, and diffuse to the surface *(Zatko et al., 2013)*. Meusinger et al. (2014) followed Davis et al. (2008) to decipher the quantum yield of nitrate photolysis and described the microphysical properties of the region around the nitrate chromophore affecting its dissociation *(Meusinger et al., 2014)*. The nitrate contained in the photo-labile domain is consumed first, being more available than the buried nitrate, hindered by a cage effect. Bock et al. (2016) developed a nitrate air-snow exchange model and tested it against the summer observations at Dome C, which demonstrated that co-condensation, the simultaneous condensation of water vapor and trace gases at the air–ice interface, was the most important

process to explain nitrate incorporation in snow *(Bock et al., 2016)*. Bock et al. (2016) model works well at cold sites on the Antarctic Plateau, where air temperatures are below the freezing point year-round and no snow melt occurs. However, the model does not reproduce the summer observations at the coast, where the temperature, relative humidity and concentration of atmospheric aerosol are much higher than that in the Plateau where snow surface melt is possible. Chan et al. (2018) developed a new model and concluded that winter air-snow interactions of nitrate between the air and skin layer snow can be described as a combination of non-equilibrium surface adsorption and co-condensation on ice, coupled with solid-state diffusion inside the grain, similar to Bock et al. (2016). Chan et al. (2018) were able for the first time to reproduce the summer observations on the Antarctic Plateau and at the Coast, concluding it is the equilibrium solvation into liquid micro pockets, based on Henry's Law, that dominates the exchange of nitrate between air and snow *(Chan et al., 2018)*.

In order to overcome the lack of knowledge related to the snow-contained nitrate photolysis, current models simulate large ranges of snow-sourced flux of nitrogen (F_{NO_x}): (0.01 – 6.4) x 10^8 molec cm^{-2} s^{-1} in Antarctica and (0.5 – 11) x 10^8 molec cm^{-2} s^{-1} for Greenland *(Huang et al., 2017; Zatko et al., 2016)*. To date, no consensus can be found in the literature about the different forms of nitrate that would allow us to reduce the modeled F_{NO_x} ranges. The disparity of existing F_{NO_x} observations and modeling in Arctic and Antarctica are quite large. Indeed, in Artic, NO_x fluxes from 2.5 to 28 x 10^8 molecules cm^{-2} s^{-1} were found, measurements and models together. F_{NO_x} measurements in Antarctica range from 1.3 to 42.5 x 10^8 molecules cm^{-2} s^{-1} while model-derived fluxes are found to be ranging from 3.2 to 22 x 10^8 molecules cm^{-2} s^{-1} *(Bauguitte et al., 2012; Beine et al., 2002; Frey et al., 2013b, 2015b; Honrath et al., 2002; Jones et al., 2001, 2011; Masclin et al., 2013; Oncley et al., 2004; Wang et al., 2007; Zatko et al., 2013)*. A major difficulty encountered for the F_{NO_x} estimation is that it depends upon two components: transport (both inward and outward of the snowpack) and photochemistry production. Previous field studies did not separate these two phenomena, making it nearly impossible to determine or to model the snowpack's source precisely. The difficulty to measure the NO_x fluxes is due to the rather weak NO_x gradient inside the snowpack with respect to the relatively high measurement uncertainties, the measurement itself being disturbed by re-deposition of nitrate, convection and ventilation. Flux estimates are usually calculated using above snow gradient method: Fick's Law describes how concentration gradient, $\frac{\partial c}{\partial z}$, and diffusion coefficient, K_c, of a chemical tracer relate to the diffusive flux F : $F = -K_c \frac{\partial c}{\partial z}$ *(Lenschow, 1995)*. However, photochemical production inside the snow grain can lead to another way of estimating NO_x flux. Indeed, Cotter et al. (2003) were the firsts to observed NO_x production rates using a laboratory flux chamber (FC) experiment. NO_x production rates under different temperatures and UV irradiations conditions lead to the determination of the mechanism involved in NO_x release from snow. These experiments did not exactly represent the Antarctic snowpack behaviour as they were carried out under artificial and controlled laboratory conditions *(Cotter et al., 2003)*. This context motivated us to conduct flux chamber experiments on the Antarctic plateau, at Dome C, during the 2019–2020 campaign. Flux chambers (FC) are the most widely used equipment to quantify gaseous emissions from solid or liquid surface sources *(Besnard and Pokryszka, 2005; Cotel et al., 2015; Pokryszka and Tauziède, 1999; Verginelli et al., 2018)*. They are widely used nowadays to assess emissions of pollutants into the atmosphere from the surface *(Scheutz et al., 2008; Sihota et al., 2010; Tillman et al., 2003)*. A dynamic FC method developed to measure emission rates from hazardous waste sites employs an inert gas that is continuously introduced at a

controlled rate. An equivalent amount of gas is allowed to leave the chamber *(Eklund, 1992)*. In our Antarctic experiments, we adapted this method for NO_x monitoring, using an open circuit FC with clean air injected and NO_x-bearing air at the outlet of the chamber analyzed, similar to Cotter et al. (2003) laboratory FC experiment. Such experiments, carried out under environmental conditions as realistic as possible, allow us to measure an integrated parameter, $\overline{J_{NO_3}}$ the daily nitrate photolysis rate constant, without being affected by the aforementioned disturbing processes, leading to a better characterization of the nitrate photolysis and its relation to NO_x emissions.

Here we explore the dynamical method of FC experiments and its robustness to better estimate the snow-contained nitrate photolysis and the related NO_x snow-pack emissions. In Section 2 we provide details of the experimental studies undertaken. In Section 3 we described the data validation process applied. In Section 4 we present the results and evaluate the impact of this method on the NO_x fluxes estimates at Dome C and extrapolated over the Antarctic continent. In section 5, we compare experiment outputs with a simple 1-D modeling case study using our observations and lastly, we provide conclusions in Section 6.

2. Methods

2.1. Site description

The flux chamber experiments were conducted from December 10th to January 7th at the French-Italian station Concordia, Dome C (75°06'S, 123°20'E, 3233m a.s.l) during the 2019-2020 campaign. In this region, the station is plunged into the polar night during the austral winter. The sun remains below the horizon from May to August while in summer (November to January) the solar zenith angle (SZA) does not go above 52° (i.e., lower than 38° above the horizon).

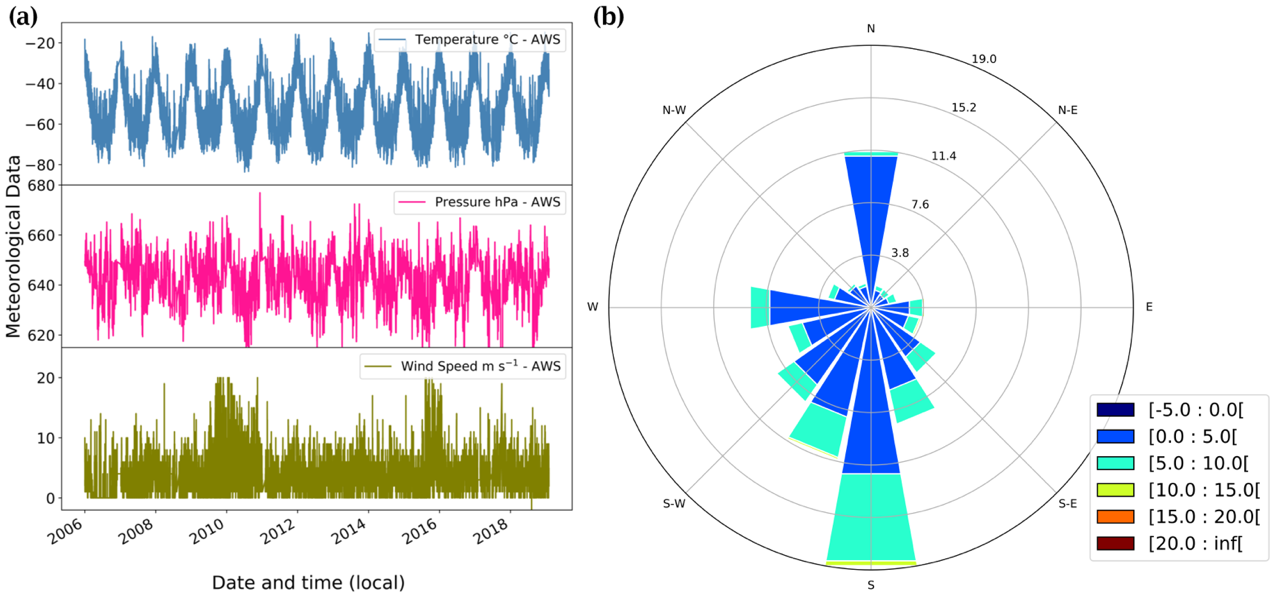

Figure 1: (a) *Multiyear meteorological observations records at Dome C, Concordia station, Antarctica measured by the local automatic weather station (AWS– Vaisala Milos 520) and* ***(b)*** *the corresponding wind rose in m s^{-1} during the period of 2006-2019. The time is given as local time (UTC + 07:00) where local solar sun maximum is noon.*

The annual climate at Dome C is mainly cold and dry (T_{mean} = - 53 ± 14 °C), typically with clear skies or elevated cirrus clouds *(Palchetti et al., 2015)*, light winds ($W_{speed\text{-}mean}$ = 3.3 ± 2.1 m s^{-1}) and low atmospheric pressure (P_{mean} = 641 ± 27 hPa), as shown in Figure 1a. These conditions are due to a dry and cold prevailing wind that comes from the south ($W_{dir\text{-}mean}$ = 172 ± 90 °), depicted in Figure 1b, as well as being on a dome of high altitude with an albedo close to 1. Summer is warmer and more humid than the annual mean, and conditions encountered during the 2019–2020 FC experiments were unexceptional compared to the typical summer climatology observed at Dome C: T_{mean} = -29 ± 5 °C; P_{mean} = 655 ± 3 hPa; $W_{speed\text{-}mean}$ = 3.1 ± 1.5 m s^{-1} and $W_{dir\text{-}mean}$ = 173 ± 80 °. More information about the meteorological conditions encountered during the experiments can be found in the supplementary material (SI 1.1).

2.2. Experiment Location and Setup

The experiment is located in the station's clean area sector, about 1 km south-west and upwind of the main station buildings (Fig. 2) in a zone less subjected to pollution linked to the activities taking place at Concordia since 1997. A container buried under the snow at the limit of the clean area and maintained at 8 °C was used to host the measuring instruments and all the equipment necessary for the experiments.

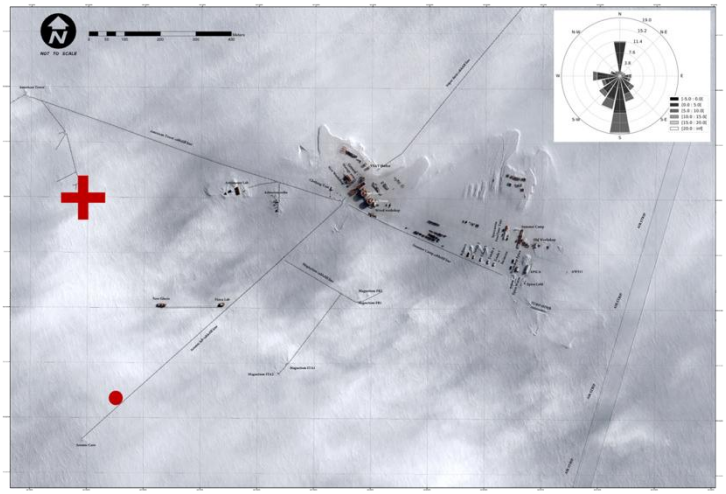

Figure 2: *Aerial view of the station: the red cross marks the position of the experiments and the red dot the location of the automatic weather station (AWS– Vaisala Milos 520). The dominant wind rose is shown in the upper right-hand corner.*

The FC experiments were designed in order to work as close as possible to natural conditions (natural snow, radiation, temperature, actinic flux and environmental conditions). They allowed the study of several types of snow. Indeed, by controlling the transport component mentioned in the introduction, the NO_x production can be estimated through Equation (1):

$$P_{NO_x} = J_{NO_3}[NO_3^-] \qquad (1)$$

where P_{NO_x} is the NO_x production (molecules s^{-1}); J_{NO_3} (s^{-1}) is the photolysis rate constant of the snowpack nitrate and $[NO_3^-]$ (molecules) is the initial amount of nitrate contained in the snow. Therefore, the objective was to study the NO_x emissions from different snows, i.e., varying $[NO_3^-]$, and the associated diurnal cycles, i.e., varying J_{NO_3}. Although the nitrate photolysis reactions (R1 to R3) produce both NO and NO_2, due to the zero-air injection, the NO:NO_2 ratio has no meaning and it is therefore more relevant to report NO_x. To that end, this study focuses on the sum of NO + NO_2 = NO_x.

NO_3^- + hν → NO_2 + O^- (R1)

NO_3^- + hν → NO_2- + $O(^3P)$ (R2)

NO_2^- + hν → NO + O^- (R3)

Because photolysis of nitrate in snow occurs under UV radiation (λ > 300 nm), UV-transparent chambers are essential for the experiment. The most UV-transparent material after glass is polymethyl methacrylate (PMMA). It is lighter than glass and more practical to use in the field; however, it gets very brittle in cold environment. Several PMMA materials were tested to find the best compromise between thickness and UV transparency. We found that a thickness of 8 mm offered general robustness and cold resistance while

keeping the weight of an empty chamber reasonable for handling in the field (~ 5 kg). Within the different PMMAs, the Plexiglas Clear GS2458 GT (EBLA-GmbH Kunststofftechnik) provided the best transparency: > 71 % of transmitted light for λ > 305 nm (transmission spectra provided in the supplementary material, SI 1.2). The chamber dimensions (70 x 21 x 21 cm) give a volume of ~ 0.03 m^3 and a total surface area of ~ 0.62 m^2, which permits enough NO_x production to be detected by the monitoring instruments.

Because light attenuates quickly with depth in the snowpack following an exponential decrease, this makes the first few centimeters of the snow column to dominate the availability of photons for photo-chemical reactions in the UV *(Brandt and Warren, 1993; Domine et al., 2008; Simpson et al., 2002)*. At Dome C, the radiative transfer model developed by Libois et al. (2013, 2014) predicts a 95 % loss of light in the snowpack after 50 cm depth at λ > 305 nm *(Libois et al., 2013, 2014)*, which represents the photic zone *(Erbland et al., 2013)*. The total snow photic zone is also typically defined as 3 times the *e*-folding depth *(Thomas et al., 2011; Zatko et al., 2016)*. We chose a chamber depth that covered one *e*-folding depth for all our snow samples, representing ~ 63-78 % of NO_x produced in the snow column. Thus, our chamber was totally immersed in the photic zone even though the vast bulk of NO_x production happens near the snow surface. The chamber was filled with snow and closed with clamps, allowing the snow to be changed and weighed easily. It was then connected to a zero-air flow at the inlet and to the analysis instruments at the outlet using ¼" (diameter ~ 0.64 cm) Teflon® tubing and connectors. The sample inlet and outlet tubes were protected from solar radiation and kept 2 to 3 °C above ambient temperature to avoid any condensation occurring inside the lines. The chamber was then buried in the snow, with the surface matching the snowpack surface, to ensure the most natural experimental conditions (Fig. 3 – further details can be found in SI 1.2). The zero-air flow was produced by pumping outdoor air through two serial zero-air cartridges connected in series (TEKRAN, 90-25360-00 Analyzer Zero Air Filter) and pushed into the FC at 58 ± 17 cm^3 s^{-1} (3.50 ± 1.05 splm) leading to a 277 ± 92 s residential time (~ 3 to 7 min). The NO_x chemical lifetime in an open atmosphere, where it is in contact with OH radicals, O_3 and other reactive species, has been previously calculated to be on the order of hours *(Browne et al., 2014; Kenagy et al., 2018; Valin et al., 2013)*. Therefore, NO_x chemical lifetime in the FC experiments is expected to be much longer. Indeed, NO_x lifetime ranging from 3h at noon to 7h a midnight was estimated at Dome C *(Legrand et al., 2014)*, making the observed NO_x concentrations directly proportional to the NO_x production.

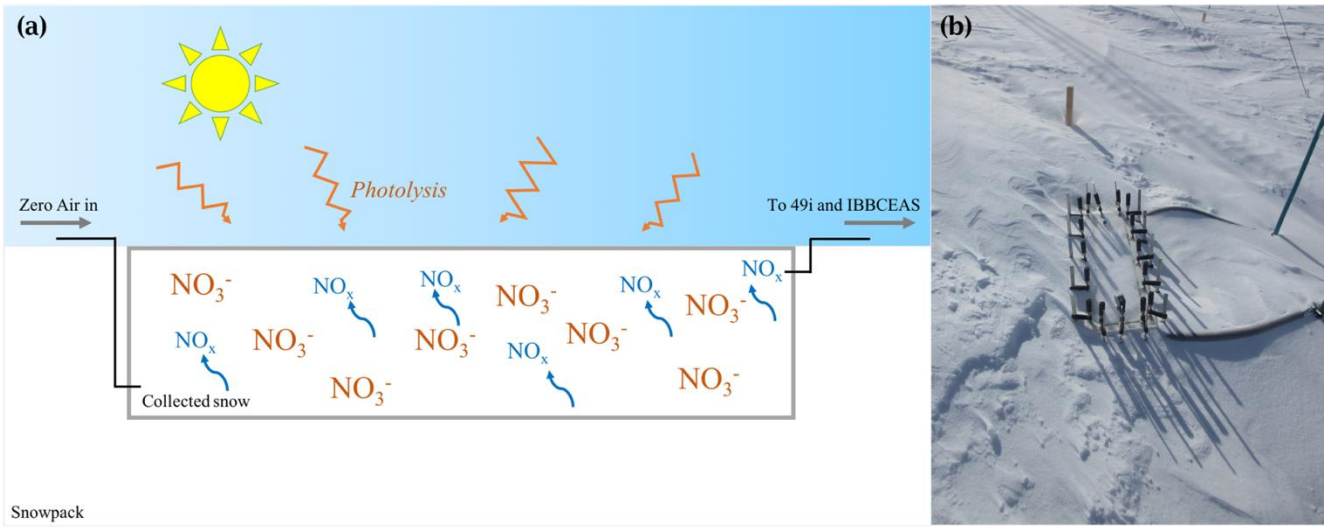

Figure 3: (a) *Schematic and* ***(b)*** *picture of one FC experiment in the field.*

2.3. Instrumentation

The twin instruments used for the NO_x detection were developed, tested and validated in the laboratory prior the campaign *(Barbero et al., 2020)*. They are based on Incoherent Broad-Band Cavity Enhanced Absorption Spectroscopy (IBBCEAS) for the detection of NO_2 in the 400 – 475 nm wavelength region. The implementation on the inlet gas line of a compact ozone generator based on water electrolysis allows the measurement of NO_x. The instruments were first calibrated using a calibrator (FlexStream™ Gas Standards Generator, KINTEK Analytical, Inc.) that produced a stable NO_2 source prior field deployment. The 10-min measurement time used during the experiments permits the acquisition of both the reference and the absorption spectra with minimum detection limits of 18 and 16 parts per trillion (ppt or 10^{-12} mol mol^{-1}) (1σ) for NO_x and NO_2, respectively, according to an Allan-Werle statistical method *(Werle et al., 1993)*, and a sensitivity on the NO_2 concentrations around 50 ppt. Field calibration was made using a NO_2 gas bottle (Air Liquide B10 - NO_2 1 ppm in N_2). The O_3 inside the chamber was monitored using a UV Photometric O_3 analyzer (Thermo Scientific, Model 49i) that achieves 0.5 nmol mol^{-1} (1σ) detection limit within 60 seconds and was calibrated with an O_3 calibration source (2B Technologies Model 306 Ozone Calibration Source™). The instrument was not dedicated to the FC experiments but was connected to a snow tower experiment *(Helmig et al., 2020)*: samples were drawn sequentially at flows of typically ~ 1-2 splm through a series of switching valves connected to each inlet line, following a 2-hour duty cycle of 8 minutes measurements on each inlet including downstream the FC. The meteorological data (Fig. 1) and information were obtained from the IPEV/PNRA Project, "Routine Meteorological Observation at Station Concordia" (http://www.climantartide.it), using an automatic weather station (AWS – Vaisala Milos 520). The UV radiation was measured with a broadband UV radiometer (Kipp & Zonen – CUV 4, spectral range 305 – 385 nm) and UV received from one experiment to the next were very similar. SZA measurements were taken from ground-based SAOZ (Système d'Analyse par Observation Zénitale) as part of the Network for the Detection of Atmospheric Composition Change (NDACC) and the data are publicly available (see http://www.ndacc.org). Flows were controlled using a piston vacuum pump (Welch™ Standard Duty WOB-L™ Piston Vacuum Pump - Model 2534C-02) and two mass flow controllers (MKS – Mass Flow Controller 10 sccm and 10,000 sccm), also used for dilution of gas source NO_2 during multi-point calibration of the IBBCEAS on the field. Nitrate concentration in snow samples from each experiment was analyzed twice in the station's laboratory with an Ion Chromatography (IC) system (Dionex™ ICS – 2000, Thermo Scientific), and snow density was calculated by gravimetry.

2.4. Sampling Strategy

Concordia is a permanent research station on the Antarctic Plateau, and scientific activities occurring in summer regularly involve vehicles, implying possible pollution. For this reason, two types of snow were collected in order to study possible spatial variability: local snow, located in the station's clean area sector (Fig. 2) and snow qualified as pristine snow, located 25 km south of the station. The same protocol was followed on each site: a pit (2 m long, 1 m wide, 1 m deep) was dug using clean shovels. The windward side was then cleaned over the entire depth of the pit. Using a small clean plastic shovel, isotherm boxes (scufa – 115 x 35 x 45 cm – cleaned prior to sampling) were filled with snow and homogenized by mixing. Each site was sampled three times at different depths: 2-7 cm, 10-20 cm and 40-50 cm for the local snow and 2-7 cm, 10-20 cm and 30-40 cm for the pristine snow. Finally, a sample of drifted snow was collected in the clean area sector the 2nd of December 2019 during a very windy episode, with wind speed of 8.07 ± 0.32 m s^{-1} (1σ) from 10:00 to 15:00 local time. Isotherm boxes containing the homogenized samples were then stored in a snow cave in the dark at constant temperature (-55 ˚C). The estimated age of each snow sample, calculated following Stenni et al. (2016) and Meur et al. (2018), is reported in Table 1 *(Meur et al., 2018; Stenni et al., 2016)*.

Table 1: *Ages of snow samples estimated from a mean snow accumulation in Dome C of ca. 25 mm per year (Stenni et al., 2016; Meur et al. 2018)*

Type of Snow	Estimated age
Drift Snow	-
2-7 cm Layer	~ 10 months to ~ 3 years
10-20 cm Layer	4 to 8 years
30-40 cm Layer	12 to 16 years
40-50 cm Layer	16 to 20 years

2.5. Typical Experiment

Prior to the experiments, the chamber was cleaned by injecting a high level of O_3 (~ 600 nmol mol^{-1}) for 12 hours followed by zero-air flushing for other 12 hours until reaching stable levels of NO_x, (0.068 ± 0.012) nmol mol^{-1}, corresponding to the chamber blank and close to the NO_2 sensitivity of the instrument (Section 2.3). The snow contained in the isotherm boxes was homogenized again and weighed once transferred in the chamber to obtain the density by gravimetry. 8.5 to 12.0 kg of snow were moved inside the chamber. The densities calculated for each experiment, ranging from 0.32 to 0.45 g cm^{-3}, agreed well with previous observations *(Gallet et al., 2011)*. A mechanical scale (TERAILLON Nautic - Pèse-personne mécanique), installed on a stable surface and leveled was used for the weighing of the snow before and after each experiment. A mean average loss of 1.1 % was measured representing about ~ 100 g of snow sample. However, the reading on this scale is accurate to ± 1 kg therefore, the losses observed are not significant in our case for the need of weight corrections. A total of eight snow samples (25 cm^3 each) were taken randomly in the chamber before the FC was sealed, for each experiment. The chamber was then buried in the snowpack, taking care to disturb the surrounding snow as little as possible, and connected to the zero-air flow. The emissions from the snow were then monitored continuously after the setup of the FC, ranging from 2 to 4 days. To investigate the possibility of nitrate stratification and denitrification during the experiments, 40 samples (25 cm^3 each) at 2 cm snow depth resolution were collected from the box after each experiment (4 samples per grid).

3. Data Processing

The NO_x measurements from the IBBCEAS were corrected from the chamber blank (0.068 ± 0.012 nmol mol^{-1}) before being further processed for validation. A 2h-running mean was calculated and the standard deviation (σ_{mean}) was determined within the same window. The data falling beyond 2 x σ_{mean} were discarded, which resulted in less than 6 % rejection. The measurements were then averaged every 20 minutes, corresponding to the best performance of the instruments to achieve the ultimate NO_x detection limit of 10 pmol mol^{-1} *(Barbero et al., 2020)*. As mentioned in Section 2.3., the O_3 inside the chamber was monitored using a UV Photometric O_3 analyzer (Thermo Scientific, Model 49i) connected by tubing to an automatic snow tower platform which housed the switching manifold and the analytical equipment. To eliminate the response time after the switching manifold, only the last three minutes of measurements, when concentrations reach steady-state, were used and averaged, giving one measurement of ozone concentration, [O_3], every 2 hours. The data were then interpolated every 20 minutes to match the resolution of the NO_x measurements. Snow nitrate concentrations, before and after the FC experiments, were disregarded when the absolute value of the measurement [NO_3^-] - [NO_3^-]$_{mean}$, was above two standard deviations (2σ) leading to 16 samples being rejected on the total of 336 samples.

4. Results and Discussions

During the seven experiments, the O_3 excess with respect to the levels expected from the photochemical $NO\text{-}NO_2\text{-}O_3$ equilibrium through the Leighton relationship *(Leighton, 1961)*, was not significant: from 0.73 to 10 nmol mol^{-1} (details of the calculations can be found in Appendix 1), therefore, we decided that there was no need to discuss the ozone data. Figure 4 shows the nitrate concentration (ng g^{-1} of snow) measured in each snow sample before and after the experiments. Drift snow was found to be up to 30 times more enriched in nitrate than the mean of all the rest of the snow samples, likely due to its high adsorption potential of nitric acid molecules enhanced by being blown and stirred by the strong wind (dark blue colors, Fig. 4). The pristine snow from the 25 km site shows a rapid decrease in nitrate concentrations with depth (red colors, Fig. 4), with less than 50 ng g^{-1} of nitrate remaining in the 30-40 cm layer while local snow shows fairly uniform concentrations over the topmost 50 cm (green colors, Fig. 4).

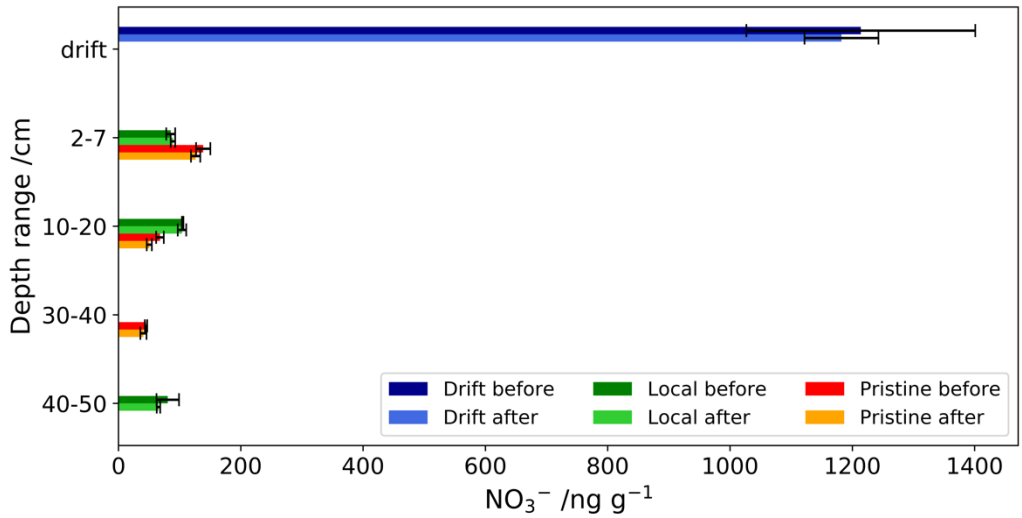

Figure 4: *Mixing ratio of NO_3^- contained in the snow (ng g^{-1}) at the two sampling sites before and after the FC experiments. In blue colors, the drift snow, in red colors, the pristine snow, i.e., 25 km South, and in green colors, the local snow. The error bars correspond to 1σ over samples measurements. The bottom layers at the two sampling sites don't match in depths due to a sampling error.*

The exponential decrease of nitrate concentration from the surface to depths is a common feature on the Antarctic plateau, fueled by photolysis denitrification occurring in the photic zone. And indeed, the concentrations in the 25 km South snow samples are in agreement with previous observations *(Erbland et al., 2013; France et al., 2011)*. The apparent homogeneous concentrations observed for the local snow is probably due to site pollution as demonstrated by Helming et al. (2020) *(Helmig et al., 2020)*.

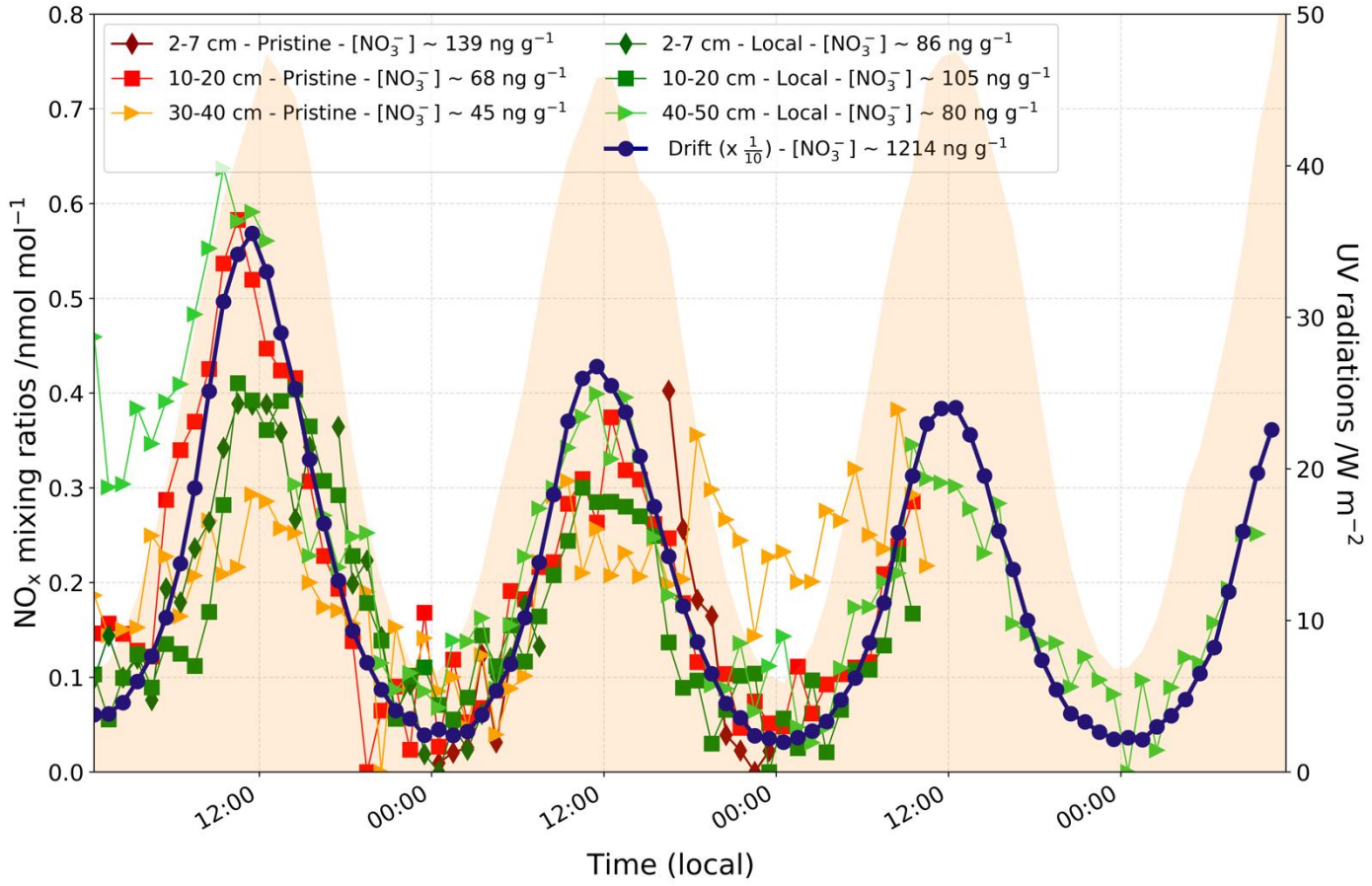

Figure 5: *NO_x gas phase mixing ratios measured downstream of the FC (nmol mol^{-1} of air), during FC experiments. Drift snow emissions (dotted blue curve) are divided by 10. Red colors represent the pristine snows, i.e., 25 km South, and green colors the local snows. The UV received during all the experiments being almost the same, shaded orange color represent the mean UV radiations over the time of the experiments measured with a broadband UV radiometer, spectral range 305–385 nm.*

Figure 5 shows the NO_x emissions monitored during the FC experiments. A strong diurnal variability in the NO_x production from the snow is observed for each experiment, with a minimum around midnight and a maximum around local noon, following the daily UV radiation cycle. A strong proportionality is observed between the nitrate concentrations contained in the snow samples and the amplitude of NO_x emissions. Secondly, an exponential decrease in NO_x emissions during the experiments is also observed. Assuming one photolyzed molecule of NO_3^- produces one molecule of NO_x (reactions R1 to R3) the denitrification occurring during the experiments represents in average (0.12 ± 0.01) % of the initial amount of nitrate, therefore negligible with respect to the initial nitrate reservoir (more details are provided in the Appendix 2). It is thus reasonable to conclude that our experiments work as pseudo-first order kinetics reaction where nitrate concentration can be assumed to be constant and NO_x emissions are driven by the photon flux only (Eq. 1). Two main patterns of temporal variations are observed for all experiments in Figure 5: an oscillation driven by the diurnal cycle of UV radiation, called steady-state regime in the following sections, to which is superimposed a slower exponentially decreasing trend with a maximum of NO_x emissions on the first day, called the transitory regime. Both regimes are being discussed separately. For the stationary regime, a comparison between the different experiments is made with the aim of better characterizing the nitrate photolysis. In a second part, the exponential decrease is studied within the same experiment in an attempt to explain the transitory regime.

4.1. Steady-State Regime Study

Flux chambers are a highly useful tool for measuring emission fluxes from local sources and their use allows us to precisely estimate emission rates. On one hand, the instantaneous NO_x production, P_{NO_x}, can be calculated based upon the measured NO_x concentrations ([NO_x]); the volume of the chamber (V_{FC}); and the residence time of the molecules inside the chamber (τ) Equation (2):

$$P_{NO_{x\,(\frac{molecules}{s})}} = \frac{[NO_x]_{(\frac{mol}{mol})} V_{FC(cm^3)}}{\tau_{(s)}} \frac{P_{(atm)} Na_{(\frac{molecules}{mol})}}{R_{(\frac{cm^3.atm}{mol.K})} T_{(K)}} \qquad (2)$$

with N_A, Avogadro's Number (6.022 x 10^{23} molecules mol^{-1}); R, the gas constant (82.06 cm^3 atm mol^{-1} K^{-1}); P (atm) and T (K) taken from the meteorological conditions at Dome C (Section 2.1). Only the volume of air in the chamber should be consider when calculating the residence time, therefore the snow porosity ($n = 1 - \frac{\rho_{snow}}{\rho_{ice}}$) is involved, with ρ_{snow} the snow density (g cm^{-3}) and ρ_{ice} the ice density (0.917 g cm-3) and $\tau = \frac{V_{FC}\,(cm^3)\,x\,n}{Flow_{air}\,(cm^3\,s^{-1})}$. On the other hand, as mentioned, our experiment works as pseudo-first order kinetics reaction where nitrate concentration, [NO_3^-] is assumed to be constant and NO_x emissions, P_{NO_x}, are driven by the photolysis rate constant J_{NO_3}, following Equation (3):

$$P_{NO_{x\,(\frac{molecules}{s})}} = J_{NO_3\,(s^{-1})} V_{FC(cm^3)} [NO_3^-]_{(\frac{g}{g})} \frac{\rho_{snow\,(\frac{g}{cm^3})} Na_{(\frac{molecules}{mol})}}{M_{NO_{3\,(\frac{g}{mol})}}} \qquad (3)$$

with $M_{NO_3^-}$ = 62.0049 g mol^{-1} the molar mass of NO_3. An estimation of the maximum instantaneous P_{NO_x} at local noon for each experiment is made using Equation (2), taking the last day of each experiment as the most representative of the steady-state regime. The results for the maximum NO_x production, P_{NO_x-max} (molecules s^{-1}), as well as the results from measurements carried out at Neumayer II Atmospheric Observatory (70°38'S, 8°15'W, 40m a.s.l) in summer 1997 *(Jones et al., 2000)*, are reported in Table 2.

Table 2: *Calculated P_{NO_x-max} (molecules s^{-1}) from Equation 2 at solar noon.*

Type of snow	Nitrate content [ng g^{-1}]	$P_{NO_{x-max}}$ [x 10^{11} molecules s^{-1}]
30-40 cm Pristine	45	6.97
10-20 cm Pristine	68	5.79
40-50 cm Local	80	5.47
2-7 cm Local	86	3.02
10-20 cm Local	105	7.09
2- 7 cm Pristine	139	5.25
Drifted	1214	85.78
20 cm x 20 cm x 20 cm block*	50	0.31

* From (Jones et al., 2000)

The NO_x production of the FC experiments seems proportional to the nitrate concentration initially present in the snow samples (Table 2) as a 10 times more concentrated snow produces ~ 10 times more NO_x, with the exception of the local snow sample at 2-7 cm depth where a lower NO_x production is observed. We strongly suspect that this sample contains absorbing contaminants emitted by the station activities. The

NO_x production of snow with similar nitrate concentrations, calculated over one day, is very similar for different snow sources (Fig. 6). It can be observed that for two very different types of snow of the Antarctic Plateau, the NO_x production is very similar (green triangles and red squares, Fig. 6). However, such similarity in production does not exist when it is compared with the Neumayer experiment *(Jones et al., 2000)*, which was located on the West Coast of Antarctica but at similar latitude (70° S) as Concordia station (75 °S) (solid black circles, Fig. 6). As shown in Figure 6, daily mean NO_x production rates from snowpack photolysis are a factor of 20 higher than the values from Jones et al. (2000), which is likely induced by differences in the NO_x snow sources and photolytic mechanics, i.e., differences in radiation fluxes, between East and West Antarctica. Additionally, the conditions of the Neumayer experiment were different to what was done for this study with the FC experiments. Indeed, at Neumayer a snow block of $0.01 m^3$ was placed 1m above the snow surface, i.e., in the open air, during the measurements, therefore subjected to direct sunlight and air ventilation all around the block *(Jones et al., 2000)*. The maximum P_{NO_x} observed at Dome C was around 5.5 x 10^{11} molecules s^{-1} while Neumayer's maximum was below 0.5 x 10^{11} molecules s^{-1} for the same summer period. As mentioned previously, the major difficulty to measure the NO_x fluxes depends upon two components: transport and photochemistry production. Our FC design experiments are insensitive to the transport component. Therefore, the factor 10 observed at noon could be due, not only to the location of the snow (Coast vs Plateau, West vs East) and a different actinic flux due to different concentrations of snow impurities, but also to this transport component. Additionally, Jones et al. (2000) did not observe any change in the nitrate concentration after 50 hours of their experiment, which supports our conclusion that the nitrate reservoir in the snowpack cannot be rapidly depleted by photolysis within the realm of hours to a few days.

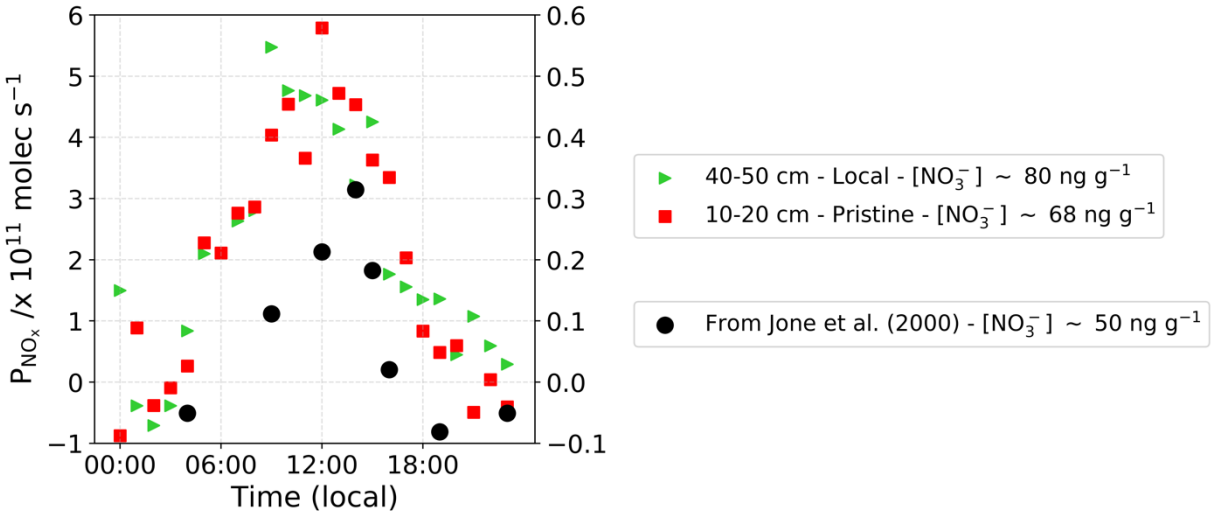

Figure 6: *Comparisons of the diurnal variability of snowpack NO_x production rates at different locations for similar nitrate concentrations snows: local snow (40-50 cm deep – Antarctic Plateau – green solid triangles), pristine snow (25 km South from Concordia station – 10-20 cm deep – Antarctic Plateau – red squares), and measurements over the Western Coast of Antarctica (black solid circles) from Jones et al. (2000).*

To estimate a daily mean photolysis rate constant, Equations (2) and (3) are combined and derived to produce Equation (4).

$$\overline{J_{NO_3}} = \frac{1}{\Delta t} \frac{\int_0^{\Delta t} [NO_x] dt}{\tau [NO_3^-]} \qquad (4)$$

where $\overline{J_{NO_3}}$ (s^{-1}) is the daily photolysis rate constant calculated from the NO_x measurements; Δt = 1 day; τ (s) is the residential time in the chamber; [NO_3^-] (molecules cm^{-3}) is the nitrate concentration of the snow sample; $\int_0^{\Delta t}[NO_x]dt$ is the NO_x concentrations (molecules cm^{-3}) integrated over one day. To estimate the NO_x concentration during the steady-state regime, a fit analysis was used for all experiments with the [NO_x] emissions following Equation (5) to smooth the measurements before evaluating the integral.

$$f(t) = a + b\ \cos(\omega t + \phi) \qquad (5)$$

where parameter a represents the fact that in summer (November to January) the sun does not go below the horizon; parameter b denotes the amplitude of the NO_x emissions; and ω and ϕ parameters are for the phase relationship. Indeed, Figure 5 shows that the NO_x emissions follow the UV radiation well, and the amount of UV itself roughly follows the cos(SZA). However, small adjustments are needed to fit to the reality of the emission. More details on the calculations can be found in the Appendix 3. A $\overline{J_{NO_3}}$ is then estimated for each experiment and results are presented in Figure 7. Measurement uncertainties for each calculated $\overline{J_{NO_3}}$ are within three times the standard deviation of the calculated values (3σ).

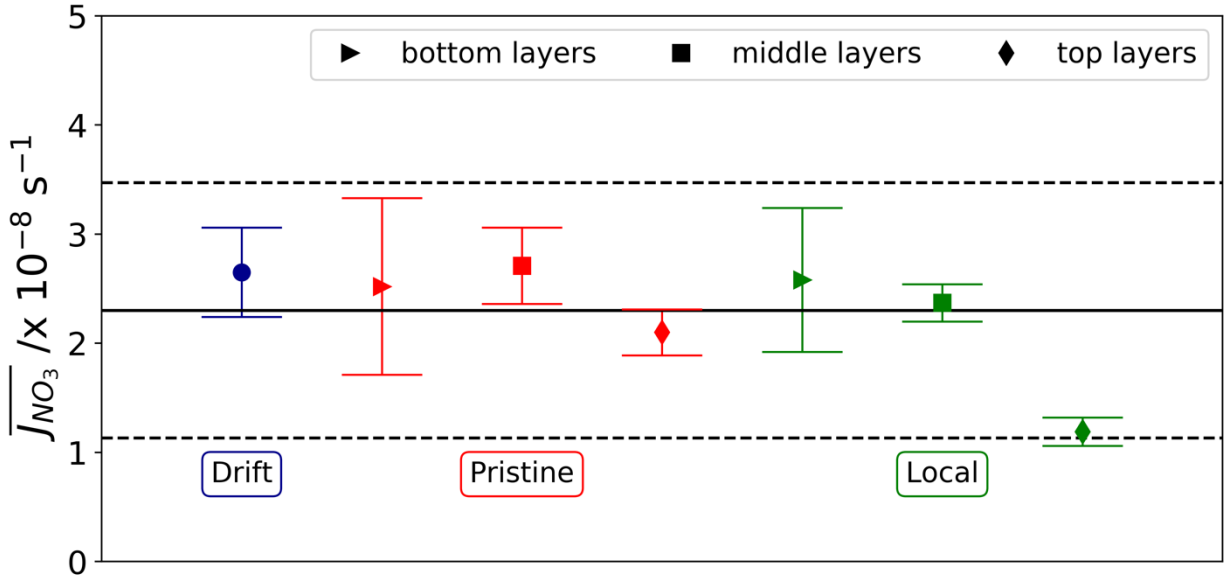

Figure 7: *$\overline{J_{NO_3}}$ for each experiment. Dark blue dot represents the drift snow, red color the pristine snow samples, i.e., 25 km South of Concordia station, and green color the local snow samples. Triangles represent the bottom layers (30-40 cm or 40-50 cm), squares the 10-20 cm layers and diamonds the 2-7 cm layers. The mean ± 3σ, calculated from all the experiments, is represented by the solid and dashed black lines.*

With the exception of the local snow sample at 2-7 cm depth suspected to have been polluted by the station activities, a mean $\overline{J_{NO_3}}$ of (2.49 ± 0.43) x 10^{-8} s^{-1} (1σ) was found for the 0-20 cm layer, to which further 37 % (i.e., e^{-1}) are added, leading to a daily $\overline{J_{NO_3}}$ of (3.94 ± 0.68) x 10^{-8} s^{-1} over the entire photic zone (0-50 cm). Those results suggest the same photolysis rate constant for different types of snow and snow ages as their $\overline{J_{NO_3}}$ range from (2.10 ± 0.21) x 10^{-8} s^{-1} (1σ) to (2.71 ± 0.35) x 10^{-8} s^{-1} (1σ). Additionally, the lifetime of NO_3^- in the chamber against loss by photolysis can be calculated as $\tau_{NO_3^-\ photolysis} = \frac{1}{\overline{J_{NO_3}}}$, *(Winton et al., 2020; Zatko et al., 2016)*, and is ranging from 1 to 2.5 years for our FC experiments, largely superior to the experiments duration.

Using the TARTES optical radiative transfer model (Two-streAm Radiative TransfEr in Snow model) *(Libois et al., 2013, 2014)* coupled with SBDART model (Santa Barbara DISTORT Atmospheric Radiative Transfer Model) *(Ricchiazzi et al., 1998)* we calculated a theoretical quantum yield to compare with our findings. The nitrate ion absorption cross section, σ_{NO3} was taken from Frey et al. (2009), σ_{NO3} = 1.2 x 10^{-20} cm^2 $molecules^{-1}$ at 305nm *(Frey et al., 2009)*. Assuming that the black carbon in the snow at Dome C varies between 1 and 5 ng g^{-1} *(France et al., 2011)* and that it represents all impurities in the model, a quantum yield ranging from 0.0057 to 0.0080 molecules $photon^{-1}$ is necessary to estimate a $\overline{J_{NO_3 modeled}}$ ranging from 3.21 x 10^{-8} s^{-1} to 4.57 x 10^{-8} s^{-1}, i.e., within the 1σ of our observed $\overline{J_{NO_3}}$. A quantum yield of NO_x from nitrate photolysis, 0.0015–0.0052 molecules $photon^{-1}$, was widely defined by Chu and Anastasio (2003) and used by Zatko et al. (2016) *(Chu and Anastasio, 2003; Zatko et al., 2016)*. Our approach allows us to reduce the range of quantum yield for Dome C. Assuming a constant nitrate reservoir as discussed previously, the NO_x production would therefore be a process only driven by the amount of nitrate accessible to photolysis. Because drift snow (young) and snow collected in depth (old) possess the same photolysis rate under the same incident light flux despite showing radically different nitrate concentrations, it can reasonably be concluded that nitrate is always accessible to photolysis with the same probability. This implies similar quantum yield, ϕ(T,pH) = 0.0069 ± 0.0016, for all snow samples (Eq. 8), which describes the availability of nitrate to photolytic loss. This contradicts with the previous studies of Davis et al. (2008) and Meusinger et al. (2014) which proposed two nitrate families: an easy photolabile nitrate (i.e., adsorbed on the surface of ice) and a more difficult to successfully photolyze nitrate population (i.e., incorporated within the ice crystal lattice). Nevertheless, our observations are in good agreement with Bock et al. (2016) and Chan et al. (2018) which proposed a single mechanism responsible for the incorporation of nitrate in the snow, at cold sites such as Dome C, among various possible mechanisms, as snowpack-induced NO_x emissions are mainly due to the nitrate photolysis *(Bock et al., 2016; Chan et al., 2018)*.

4.2. Transitory Regime Study

The transitory regime represents the decreasing exponential trend observed over the three days of the FC experiments, with a maximum of NO_x emissions the first day observed in Figure 5. NO_x emissions decrease from one day to the next. For the drift snow, $\frac{\Delta P_{NO_x}}{P_{NO_x}}$ represents ~ 22 % for day 1 to day 2 and ~ 12 % for day 2 to day 3. The total NO_x production ($P_{NO_{x-tot}}$) observed in Figure 5 can be expressed as the sum of the steady state regime production ($P_{NO_{x-steady}}$) and the transitory regime production ($P_{NO_{x-trans}}$) Equation (6). In other words, despite the conclusion of section 4.1, here, the hypothesis of two nitrate populations is made with $P_{NO_{x-steady}}$ already discussed in Section 4.1.

$$P_{NO_{x-tot}} = P_{NO_{x-trans}} + P_{NO_{x-steady}} \quad (6)$$

$P_{NO_{x-trans}}$ is calculated as a function of $J_{NO_{3-trans}}$ and $[NO_3^-]_{trans}$, following Equation (1) and expressed here by Equation (7).

$$P_{NO_{x-trans}} = J_{NO_{3-trans}}[NO_3^-]_{trans} \quad (7)$$

We hypothesize that the nitrate photolysis rate at the transitory regime ($J_{NO_{3-trans}}$) varies with time and depends on a variety of parameters represented in Equation (8).

$$J_{NO_3} = \sigma_{NO3}(\lambda)\ \phi(T, pH)\ I_{act}(\theta, \psi, \lambda, z) \quad (8)$$

where λ (nm) is the wavelength; θ the SZA; ψ marks the sun declination and z (m) is the snowpack's depth; $\sigma_{NO3}(\lambda)$ is the absorption cross section of nitrate; ϕ(T,pH) and $I_{act}(\theta,\psi,\lambda,z)$ are nitrate photolysis quantum yield and actinic flux, respectively. In this experiment, the $\sigma_{NO3}(\lambda)\,\phi$(T,pH) product is considered constant as the experiments were carried out under the full spectrum, i.e., with natural sunlight and similar temperature diurnal cycle from one day to the next during the experiments. Plus, the snow pH is considered to be around 5 and constant over those layers. Additionally, $I_{act}(\theta,\psi,\lambda,z)$ is considered only θ and ψ dependent as the measurements are integrated over the chamber's depth. There is no indication that the actinic flux varies substantially from one day to the next over the chamber's depth; thus, the radiative conditions were the same from one day to another (good weather, homogeneous snow layer, slow metamorphism) and a $J_{NO_{3-trans}}$ that varies from one day to another cannot explain the decrease in NO_x emissions observed for each experiment. This leaves the hypothesis of a strong denitrification that could describe this observation.

In Section 4.1, it has been demonstrated that the NO_x production scales with the nitrate concentration in the snow samples. Logically, a decrease in NO_x production will imply a decrease in nitrate concentrations with the same levels which is not observed (Section 2.5). Using Equation (2) from Meusinger et al. (2014), $J^* = -\ln\left(\frac{[NO_3^-]_{after}}{[NO_3^-]_{before}}\right)\frac{1}{t_{photolysis}}$, with $t_{photolysis}$ (s) the experiments duration, $[NO_3^-]$ (molecules cm^{-3}) the concentrations before and after the experiments, and J^* (s^{-1}) the apparent photolysis rate constant, calculated in section 4.1. Expected NO_3^- losses were calculated for each experiment, ranging from 0.3 to 15 ng g^{-1}, not detectable with our IC measurements as it falls within the 1σ. It is possible as well that a thin

surface layer is denitrified much faster due to a phenomenon of amplification of the photolysis in this layer, but this was not captured with a coarse sampling resolution of 2 cm either *(Traversi et al., 2017)*. Simpson et al. (2002) modelized the ratio of the in-snow actinic flux to the incident down-welling actinic flux as a function of extinction optical depth (proportional to depth for homogeneous snow) within the snowpack *(Simpson et al., 2002)*. Snow increases the actinic flux within the topmost layers of the snowpack, due to the high albedo in the UV region. The actinic flux at the snow surface is equal to the atmospheric actinic flux above the snow, whereas in the first few mm, depending on SZA, the actinic flux is either increased or decreased. For SZA = 0°, the actinic flux is enhanced by the conversion of direct light to diffuse light. Madronich (1987) argued that the maximum enhancement factor is four times higher than the incident actinic flux *(Madronich, 1987)*. Using the TARTES optical radiative transfer model, relative actinic fluxes for each snow samples at 305 nm were simulated (Fig. 8), using specific surface area (SSA) as a function of snow depth following Gallet et al. (2011) *(Gallet et al., 2011)*. No significant differences between the up-welling and the down-welling irradiance are observed (solid orange curve and dotted kaki curve, Fig. 8), making the travel of the light nearly isotropic within the snowpack, i.e., the same properties in every direction, even near the surface. It results that the actinic flux is relatively smooth and ranges between 0.6 and 2.8 times the flux received by the snowpack at 305nm for the 0-50 cm layer. This variation range is far too small to explain a localized layer with highly photolabile nitrate that would be depleted over the three days of the experiment, given the initial abundance of nitrate in all the samples. Additionally, old snows of 16-20-year-old would not experience such a transitory regime as the $\tau_{NO_3^-\,photolysis}$ for those samples were calculated to be ~1 year (Section 4.1). As the whole thickness of a snow sample undergoes the same exponential decrease, and the photolysis rate constant does not depend on the snow age nor location and that no change in nitrate concentration has been observed, it is difficult to explain this decrease from a variability of $[NO_3^-]_{trans}$ or $J_{NO_3-trans}$. Thus, we conclude that this transitory regime is potentially due to an experimental interference or artefact.

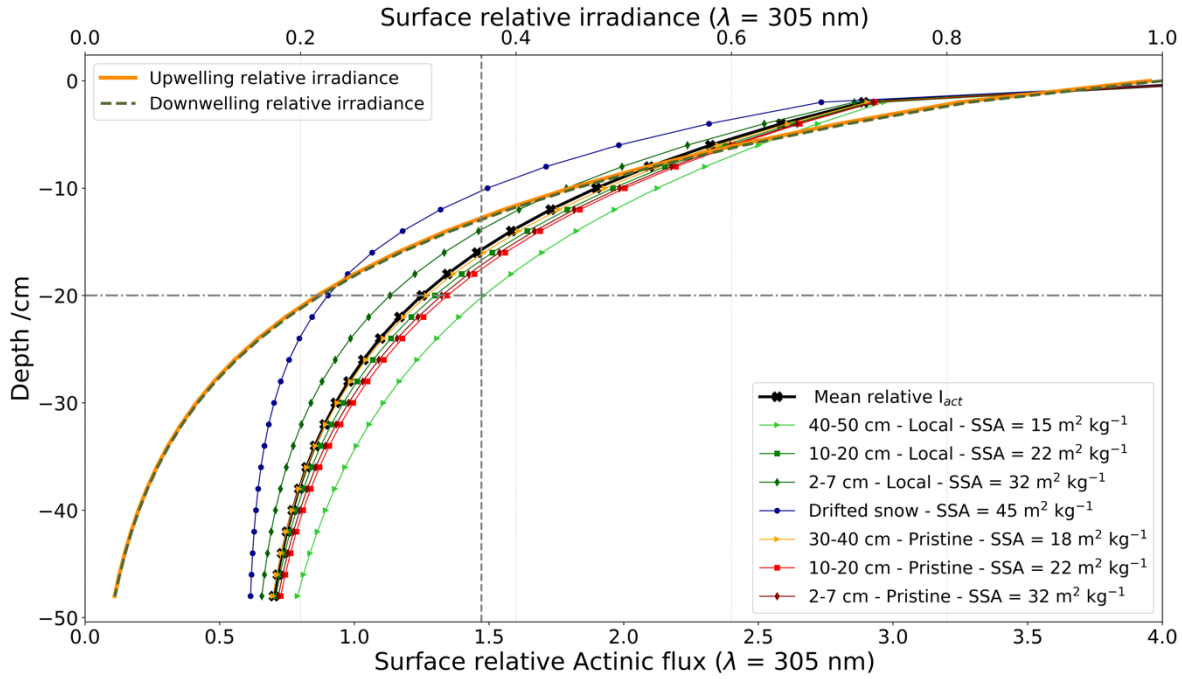

Figure 8: *Simulated surface relative actinic fluxes and irradiance for each experiment using TARTES model at 305 nm. The actinic flux describes the number of photons incident at a point, while the irradiance describes the radiant energy crossing a surface. Dotted*

horizontal line represent the depth of the chamber while the vertical dotted line represents the e-folding depth, 20 cm for the 40-50 cm local snow sample and ~ 12 cm for the drifted snow.

Another important result of the model is that the SSA cannot explain the observed difference in NO_x production between the samples, either. Indeed, at a depth of 20 cm there was a maximum difference of ~40 % between the most scattering snow (fresh snow) and the least scattering snow (old snow), lower than the observed production differences between the samples.

The adsorption of nitric acid (HNO_3) on the walls of the chamber during the installation of the experiment could be an explanation. Zhu et al. (2008) determined the absorption cross sections of surface-adsorbed HNO_3, noted $HNO_{3\text{-adsorbed}}$, in the 290-330 nm region using cavity ring-down spectroscopy. They found that the $HNO_{3\text{-adsorbed}}$ absorption cross section at 305 nm was (1.09 ± 0.17) x 10^{-18} cm^2 $molecules^{-1}$. This makes the absorption cross section of $HNO_{3\text{-adsorbed}}$ ~ 700 times higher than that in the gas phase ($HNO_{3\text{-gas}}$): (1.68 ± 0.19) x 10^{-21} *(Zhu et al., 2008)*, 1.50 x 10^{-21} *(Burkholder et al., 1993)* and 1.45 x 10^{-21} cm^2 $molecules^{-1}$ at 305 nm *(Rattigan et al., 1992)*. Burley and Johnston (1992) showed that the absorption cross section of the nitrate ion around 305 nm was 2.7 x 10^{-20} cm^2 $molecules^{-1}$ *(Burley and Johnston, 1992)*, and Frey et al. (2009) found 1.2 x 10^{-20} cm^2 $molecules^{-1}$ at Dome C *(Frey et al., 2009)*. Therefore, with a cross-section 40 to 90 times greater than that in the gas phase, the observed exponential decay could indeed be caused by the $HNO_{3\text{-adsorbed}}$ on the chamber's walls during the experiments set-up. A simple calculation giving the concentration of $HNO_{3\text{-adsorbed}}$ needed to produce the amount of NO_x observed in the transitory regime, called $NO_{x\text{-trans}}$, support this hypothesis: 0.01 to 2 pmol mol^{-1} of $HNO_{3\text{-adsorbed}}$ would be needed to produce this $NO_{x\text{-trans}}$ trend by its photolysis destruction. However, the lifetime of NO_3^- from $HNO_{3\text{-adsorbed}}$ is ranging from 60 days to over 6 years, which do not explain the short (2 to 3 days) transitory regime observed.

Another hypothesis can also be addressed: the storage of the snow samples before running the FC experiments could as well be involved. As mentioned in section 2.4, the snow samples were stored in a snow cave, in the dark and at constant temperature (-55 ˚C) for many days. Therefore, it would be possible that mobile species, with low concentration, has been diffused to the surface of grains during storage. Previous studies estimated the diffusion coefficient of HNO_3 in ice ranging from (10 to 110) x 10^{-12} cm^2 s^{-1} at -15 ˚C *(Domine and Thibert, 1995; Sommerfeld et al., 1998)*. The snow samples in their isotherm boxes were stored from 1 to 34 days at most, and the ratio $\frac{\Delta P_{NO_x}}{P_{NO_x}}$ from day 1 to day 2 seems related to the number of days it stayed in the storage cave, Figure 9a. An estimation of the distance that HNO_3 could have travelled at -15 ˚C in the snow samples during the storage is calculated using Equation (9).

$$x = \sqrt{q_i D t} \qquad (9)$$

with x (cm) the mean distance from the starting point that the molecule will have diffused in time t; q_i a numerical constant which depends on dimensionality, here $q_i = 6$ since the molecule is diffusing in every direction; D (cm^2 s^{-1}) the diffusion coefficient previously mentioned and t (s) the storage time. A range of 23-440 µm was found at -15 ˚C (Fig. 9b). With such distance at -15 ˚C, the hypothesis is probable even though at -55 ˚C diffusion is expected to be significantly slower. The rate of diffusion seems to allow such a displacement and this explanation agrees with Bock's co-condensation theory already mentioned in Section 4.1., suggesting that a single dominant incorporation mechanism is controlling the nitrate deposition in snow and explaining that a young snow will locate the nitrate in the same place as an older

snow, however, once again with a NO_3^- from $HNO_{3\text{-adsorbed}}$ lifetime larger than 60 days, this does not explain the short (2 to 3 days) transitory regime observed.

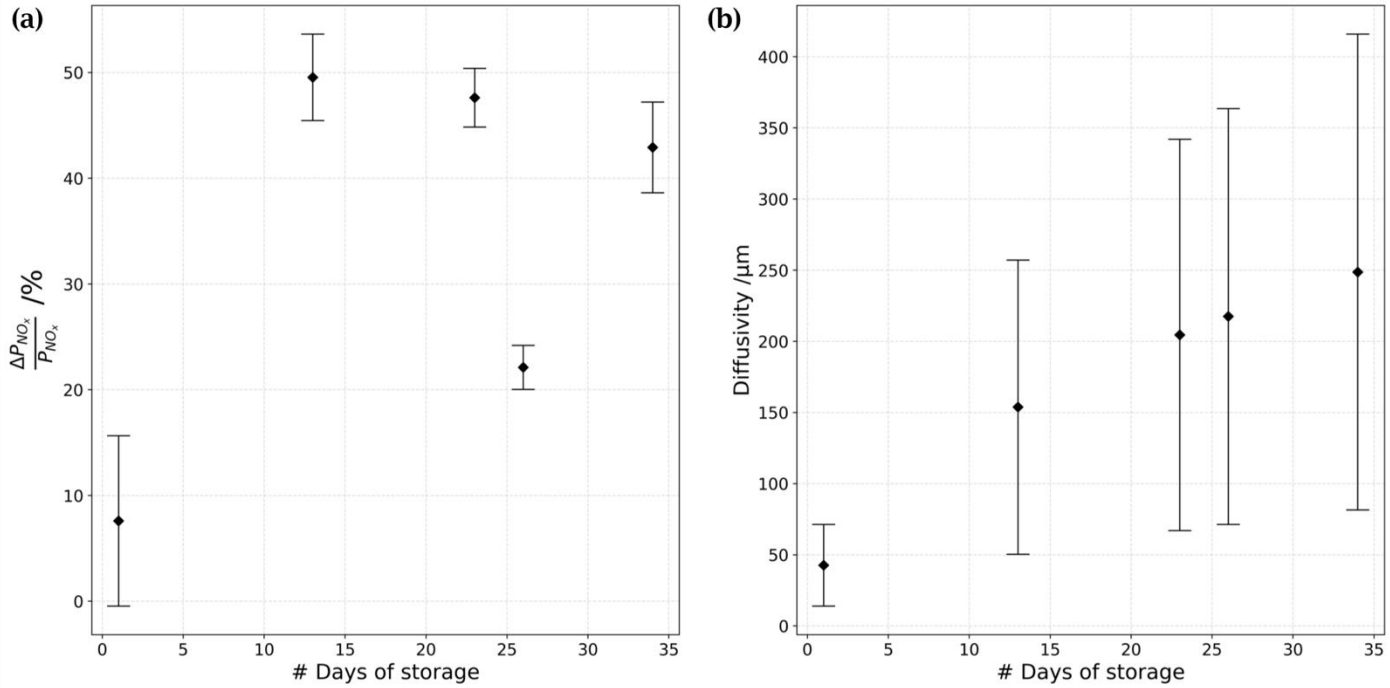

Figure 9: (a) *% of NO_x production decrease as a function of the number of days the sample stayed in storage and* ***(b)*** *an estimation of the distance (µm) that HNO_3 could have travelled in the isotherm box at -15 ˚C.*

With the available data, both theories proposed to explain the observed transitory regime, i.e., HNO_3 diffusivity or desorption in the snowpack, or HNO_3 surface adsorption during the experiments set-up, are not entirely in agreement with the observations.

One last hypothesis is the slow gas diffusivity in the firn. The observed transitory regime could be due to the leaching process of NO_x produced by nitrate photolysis prior the experiment and still present in the pores of the snow at the beginning of the FC experiment. Fabre et al. (2000) studied air diffusion in polar firns and showed that cold sites have low diffusivities *(Fabre et al., 2000)*. Indeed, Helmig et al. (2020) showed the fast penetration of NO_x in the snow during pollution events but the very slow return to background levels in the 0-70 cm layers *(Helmig et al., 2020)*. Figure 6 of the article shows that a NO_x pollution peak was evacuated of the snowpack after at least one week. Pinzer et al. (2010) studied the diffusion of NO_x and HONO in snow and found effective diffusivity of ~ 1.30 x 10^{-5} m^2 s^{-1} for both NO and NO_2 at ~ -30 ˚C *(Pinzer et al., 2010)*. However, their experiments used snows with lower density than ours and the storage of their sample was made at higher temperature. Those differences are leading to lowest expected diffusivity for our snows and are strengthening our theory. However, more experiments with different storage times and longer NO_x gas phase mixing ratios monitoring may be helpful to quantify that phenomenon with less uncertainties.

4.3.NO_x Flux Estimates and Implications on the Antarctic Plateau

By using open circuit FC with clean air flow injection, instantaneous production can be measured and an estimated average daily production can be obtained. The next step is to estimate the flux per unit of surface area. In this section, NO_x flux is estimated at Dome C and an extrapolation to the entire Antarctic continent is proposed in order to obtain a continental N-budget.

4.3.1. Estimated NO_x Flux at Dome C during the observation period

NO_x flux is defined as the NO_x production per surface unit. From Equations (2) and (3), the production was estimated for each experiment and a constant daily $\overline{J_{NO_3}}$ of (2.49 ± 0.43) x 10^{-8} s^{-1} (1σ) was found for a 20 cm snow thickness. In order to estimate the NO_x flux during the observation period at Dome C, Equation (10), a representative NO_3^- concentration in the snowpack is needed. Monthly snow pits at Dome C have been sampled for several years through the programs NITEDC and CAPOXI. A total of 33 snow pits taken at Dome C during the summer months from 2011 to 2019 were averaged to match the observation period of the FC. This provided a robust estimate of the nitrate concentration in the first 20 cm of the snowpack for Dome C: 143 ± 28 ng g^{-1}.

$$F_{NOx} = \frac{\overline{J_{NO_3}}[NO_3^-]V_{FC}}{S_{FC}} \qquad (10)$$

with $\overline{J_{NO_3}}$ (s^{-1}) the daily photolysis rate constant, [NO_3^-] (molecules cm^{-3}) the nitrate concentration of the photic zone, S_{FC} = 6,200 cm^2 the chamber's surface, and V_{FC} = 26,500 cm^3 its volume. With a snow density of 0.339 ± 0.001 g cm^{-3} for a 0-20 cm layer *(Gallet et al., 2011)*, a daily F_{NOx} of (5.0 ± 2.7) x 10^7 molecules cm^{-2} s^{-1} has been calculated for the 0-20 cm layer. As mentioned in Section 2.2, 20 cm corresponds to approximately one e-folding depth. Therefore, to extend the F_{NOx} estimation to the entire photic zone, further 37 %, i.e., e^{-1}, should be added to the previous calculations, leading to a daily F_{NOx} of (7.9 ± 4.3) x 10^7 molecules cm^{-2} s^{-1}. Table 3 compares the results of this study with previous observations made on the Antarctic Plateau: South Pole and Dome C.

Table 3: *Daily NO_x Flux estimates from observations on the Antarctic Plateau*

References	Daily F_{NO_x} [x 10^8 molecules cm^{-2} s^{-1}]	$\overline{J_{NO_3}}$ [x 10^{-8} s^{-1}]	Observations Period	Location
Oncley et al. (2004)	3.9 ± 0.4	-	26-30/11/2000	South Pole
Frey et al. (2013)	6.6	-	23/12/2009 - 12/01/2010	Dome C
Frey et al. (2013)	8.2 ± 7.4	-	22/12/2009 - 28/01/2010	Dome C
Frey et al. (2015)	9.4	-	01-08/12/2011	Dome C
Frey et al. (2015)	31	2.93	09-22/12/2011	Dome C
Frey et al. (2015)	13	2.68	23/12/2011 - 12/01/2012	Dome C
This work (2020)	0.79 ± 0.43	3.94 ± 0.36	10/12/2019 - 07/01/2020	Dome C

Snowpack NO_x emissions have been estimated to be ~ 5 to 40 times higher than what is estimated here with a daily photolysis rate constant approximately 1.5 times greater than that used by Frey et al. (2013, 2015) and estimated using models *(Frey et al., 2013a, 2015a)*. Therefore, the large discrepancies observed on the F_{NOx} estimate seem to be related to the uncertainty of the transport component, manifested by a

reduction of the uncertainties up to a factor of ~ 20. Table 4 hereafter sums up some of the daily average $\overline{F_{NO_x}}$ derived from field observations and models at both poles. The disparity of existing $\overline{F_{NO_x}}$ observations and modeling in Arctic and Antarctica are quite large.

Table 4: *Polar NO_x net fluxes measured above the snow surface in molecules cm^{-2} s^{-1}*

	Direct measurement				Model-derived			
	$\overline{F_{NO_x}}$ [x 10^8 molecules cm^{-2} s^{-1}]	Period	Site	Ref	$\overline{F_{NO_x}}$ [x 10^8 molecules cm^{-2} s^{-1}]	Period	Site	Ref
Antarctica	1.3	Feb. 1999	Neumayer	Jones et al. (2001)	3.2 - 4.2	Dec. 2003	South Pole	Wang et al. (2007)
	3.9 ± 0.4	Nov. 2000	South Pole	Oncley et al. (2004)	3.2 - 17	Jan.	Dome C	M. C. Zatko et al. (2013)
	2.42 ± 50 %	Jan. 2005	Halley	Jones et al. (2011)	3.3 - 22	Jan.	South Pole	M. C. Zatko et al. (2013)
	1.7	Summer 2005	Halley	Bauguitte et al. (2012)	3.5	Summer 2005	Halley	Bauguitte et al. (2012)
	8.2 ± 7.4	Jan. 2010	Dome C	Frey et al. (2015)				
	25 ± 8	Dec. 2011	Dome C	Frey et al. (2013)				
	42.5	Dec. 2008	WAIS Divide	Masclin et al. (2013)				
	0.79 ± 0.43	**Dec. 2019**	**Dome C**	**This work**				
Arctic	2.5	Summer 2000	Summit	Honrath et al. (2002)	13 - 28	Jan.	Summit Pole	M. C. Zatko et al. (2013)
	≥ 6.7	Apr. 2004	Alert	Beine et al. (2002)				

However, we report for the first time $\overline{F_{NO_x}}$ estimate using FC approach and giving fluxes less than 1 x 10^8 molecules cm^2 s^{-1}.

4.3.2. Annual NO_x budget extrapolated to the continent

The chemical reactivity of the snowpack and its connection to the overlying oxidative atmosphere is key to understand how it influences the polar environment. A better estimation of the interactions between the snowpack and NO_x emissions offers the perspective of quantifying its importance on a continental scale. Several studies agree that nitrate concentrations in the Antarctic snowpack are generally constant from the coast into the plateau *(Becagli et al., 2004; Erbland et al., 2015; France et al., 2011; Shi et al., 2018; Winton et al., 2020)*. Therefore, the average [NO_3^-] measured at Dome C on the 0-50 cm layer, 108 ± 8 ng g^{-1}, can be taken as a fair approximation for the entire Antarctic continent (more information in the Appendix 4). To estimate an annual N-budget for the continent, the daily production of NO_x must be calculated for each day of the year. As shown by Equation (8), J is also a function of SZA, θ, affecting the position of the sun over the year, and the sun declination, ψ, controlling the length of the day of each day over the year. The term ψ, difficult to be analytically resolved *(Finlayson-Pitts and Pitts, 2000)*, can be approached by calculating it relatively to a reference day, in our case, the 30th of December. By using the ratio $L_{day\text{-}i}$:$L_{day\text{-}ref}$ with $L_{day\text{-}i}$ being the day duration of a day of interest and $L_{day\text{-}ref}$ the length of the reference day (more details on the calculation are found in the Appendix 5). Additionally, the variability of the SZA, associated to the maximum amplitude of the NO_x emissions, should be considered in the extrapolation and it is represented here by a cosine ratio of the solar noon sun's position for the day of interest over the one of reference, i.e., December 30th. This calculation is deduced by Equation (11) hereafter *(Finlayson-Pitts and Pitts, 2000; Forsythe et al., 1995)*.

$$P_{NO_x-year} = [NO_3^-]_{mean} V_{cont} \sum \overline{J_{NO_{3-ref}}} \frac{L_{day-i}}{L_{day-ref}} \frac{\cos(\theta_i)}{\cos(\theta_{ref})} \qquad (11)$$

θ_i is taken from NDACC and $\overline{J_{NO_{3-ref}}}$ is taken from the observations on a 0-20 cm layer: (2.49 ± 0.43) x 10^{-8} s^{-1} (1σ). Further 37 % (i.e., e^{-1}) are added to the annual NO_x production to cover the entire photic zone (0-50 cm). The annual Antarctic continent NO_x budget from the nitrate snow source calculated from Equation

(11) is (0.193 ± 0.065) Tg(nitrate) y^{-1}, or (0.045 ± 0.015) Tg.N y^{-1}. This is a small source on a global scale compared to other natural sources, such as biomass burning (7.1 Tg.N y^{-1}), soil (5.6 Tg.N y^{-1}) or lightning (5.0 Tg.N y^{-1}) *(Ehhalt et al., 2018)*. Nevertheless, this comparison on a continental scale with another nitrogen source, such as the stratosphere denitrification, is more useful to understand its significance. Indeed, the evidence for denitrification in the Antarctic stratosphere is well established since the 90s *(Deshler et al., 1991; Fahey et al., 1990; Mulvaney and Wolff, 1993; Salawitch et al., 1989; Santee et al., 1995; Van Allen et al., 1995)*. Savarino et al. (2007), quantified the corresponding injection of HNO_3 into the troposphere: the additional concentration in the tropospheric reservoir was calculated to be (341 ± 141) ng m^{-3} (gaseous plus particulate nitrate) *(Savarino et al., 2007)*. Denitrification extends to an area over the entire Antarctic continent (14 million km^2), and a mean height of the atmosphere of 7.4 km. They estimated a N-budget of (0.035 ± 0.015) Tg(nitrate) y^{-1} or (0.008 ± 0.003) Tg.N y^{-1} coming from the stratosphere denitrification, more than five times less the N-budget of the snowpack denitrification estimated here, making the snowpack source a rather significant source. However, the nitrate loss by snowpack denitrification cannot be greater than the stratospheric nitrate source, therefore, another source of nitrate dominating the stratospheric source is required to explain this observation. Another element of comparison is the N loss by ice loss. During the period of 2009-2017, the total mass loss of ice of the Antarctic continent was calculated to be 252 ± 26 Gt y^{-1} *(Rignot et al., 2019)*. With an average nitrate concentration of 108 ± 8 ng g^{-1}, the continent would be losing 0.027 ± 0.005 Tg(nitrate) y^{-1} or 0.006 ± 0.001 Tg.N y^{-1}. Throughout the period studied by Rignot et al. (2019), the mass loss was concentrated in areas closest to warm, salty, subsurface, and circumpolar deep water (CDW), resulting in the melting of floating ice shelves and the destabilization of glaciers. From this comparison, it appears that the loss by glaciers is roughly equivalent to the stratospheric nitrate source.

Therefore, two scenarios are conceivable: i) all the NO_x produced by the snowpack denitrification are re-oxidized, making the balance null and closing the nitrate budget in Antarctica; ii) photolysis destruction of snow nitrate is potentially the dominant denitrification factor of the Antarctic cryosphere and another source, such as long-range transport in the troposphere is necessary to compensate this loss.

That said, note that this extrapolation to the continent is still a rough one as it does not consider the differences on the e-folding and the quantum yield variations with temperature and pH. Indeed, very recently, Noro and Takenaka (2020) showed that at a coastal site located approximately 100 km away from the Japanese Syowa Station in East Antarctica, a site called H128 (69°23'S, 41°34'E), 50 % of the nitrate on surface snow is lost by photolysis and 20 % of the nitrate is absent at 40 cm deep. Additionally, they suggest that a photic zone of 45 cm depth is observed at a low impurity Coastal site such as H128, making the photic zone at the coast close to the one observed at the Plateau *(Noro and Takenaka, 2020)*. Ideally, a 3-dimensional global chemical transport model of this snowpack source, with more FC experiments done at strategic points of Antarctica will be able to answer this question as NO_x production, deposition and exportation depend also on latitude, transport and photo-oxidative recycling of NO_x to nitrate and vice versa.

4.4. 1-D model case study

In order to understand the impact of these NO_x emissions fluxes on the boundary layer concentrations, we have completed a 1-D model case study for Dome C between the 22nd - 23rd January 2020. An hourly NO_x flux ($F_{NOx\text{-}hourly}$) for this period was calculated by applying the same method used to determine the daily J_{NO_3} and F_{NOx} values described in Section 4.3.1. We implemented and tested this $F_{NOx\text{-}hourly}$ using a one-dimensional atmospheric chemistry and transport model, PACT-1D, and simulated the NO_x mixing ratio at 1 meter above the surface snow. A full description of the 1D model has been detailed in *(Tuite et al., in review)* but is briefly summarized here. Chemical kinetics and vertical transport processes are calculated online in the model driven by the local meteorology. The regional climate model MAR, which has been applied extensively for studying the polar regions *(e.g. Agosta et al., 2019; Gallée et al., 2015; Gallée and Gorodetskaya, 2010)*, was used in its latest Antarctic configuration (version 3.11; *(Kittel et al., 2020)*) including drifting-snow physics *(Amory et al., 2020)* at 35 km resolution and forced by ERA5 reanalysis to generate the driving meteorology (3-hourly wind speed, temperature and relative humidity) extracted from the closest grid point to the measurement location. Photolysis rates are input using the Tropospheric Ultraviolet and Visible (TUV) radiation model *(Madronich and Flocke, 1999)*, and vertical eddy diffusivities (Kz) are calculated based on the parameterization described in *(Cao et al., 2016)*. Using the $F_{NOx\text{-}hourly}$ derived from the observations, we added an emission flux of NO_2 to the lowest level in the model to simulate snowpack NO_x emission between the dates of 22nd and 23rd January 2020 (BASE run). The first 17 hours of the 22nd January were used as model spin up and are excluded from the analysis. During this spin up period, the emissions were adjusted to ensure initial NO_x concentrations for our case study were representative of the initial values measured at 1 meter.

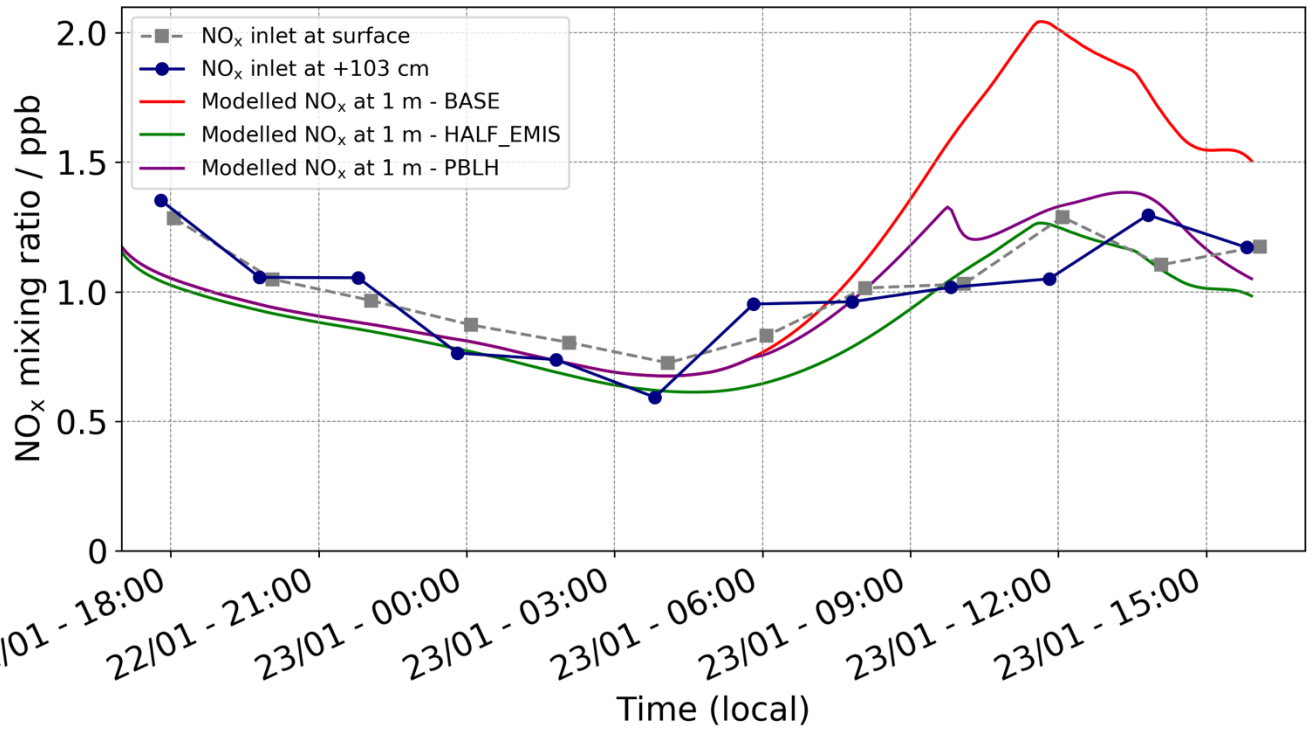

Figure 10: *Modelled NO_x mixing ratios at Dome C between the 22nd - 23rd of January 2020, at 1 m above the snow surface. Model runs BASE (red), HALF_EMIS (green) and PBLH (purple) are plotted with the observations at the snow surface (grey) and at 1 m (navy).*

The model simulated NO_x mixing ratio at 1 m above the surface and the observed NO_x time series at the snow surface and at 1 m for the same period are shown in Figure 10. Starting at 17:00 local time on 22/01/20, both the model and the measurements show a steady decline in NO_x during the period with reduced sunlight, which decreases the photochemical source of NO_x from the snowpack. Slow NO_x losses during the evening hours include conversion to HNO_3, NO_x deposition to the snow, and loss to aerosols. In the morning hours, when solar radiation is greater and NO_x fluxes increase, the concentrations within the boundary layer increase more quickly in the model than in the measurements. The 1D model results show that NO_x is overestimated during the day, which may be due to one of two main factors that influence modeled NO_x: boundary layer dynamics (boundary layer heights/vertical mixing) and emission fluxes. Here we test which of these two factors can explain the disagreement in model predicted and measured NO_x during the day. To do this we performed two sensitivity runs, one with reductions to the estimated $F_{NOx\text{-}hourly}$ (HALF_EMIS) and the other with increases to the daytime boundary layer height (PBLH). With no differentiation possible between the primary emissions of NO_2 and NO from the flux chamber experiments, interconversion between the species in the snowpack is therefore not possible to account for and so we performed the HALF_EMIS run considering half the total $F_{NOx\text{-}hourly}$ as NO_2 emissions. The PBLH run was performed to test uncertainties in the boundary layer dynamics and used a daytime (06:00-16:00) boundary layer height of approximately twice the values used in the BASE run (see Figure 3.2.3 in the supplementary material). The results from both of these sensitivity runs show a marked reduction of the daytime NO_x levels and are both in closer agreement with the observations. These results show that both factors are significant in modelling NO_x close to the surface and that both factors can, in part, explain the disagreement between the BASE model run and observations. Further quantification of these uncertainties would require additional measurements to treat NO and NO_2 separately as well as improved estimates of the boundary layer height from detailed turbulence measurements. Future modelling studies could also be performed to test the NO_x fluxes presented in this work under different meteorological conditions.

5. Conclusion

Flux chambers experiments carried out from December 10th to January 7th during the 2019-2020 campaign at Dome C, Antarctica, improved our understanding of the mechanics of snow-contained nitrate photolysis. Unexpectedly, a common daily average photolysis rate constant of $(2.49 \pm 0.43) \times 10^{-8}$ s^{-1} (1σ) was estimated for different types of snow samples (different ages and locations) on a 0-20 cm layer. This finding suggests that the photolyzable nitrate present in the snow acts as a uniform source with similar photochemical characteristics such as quantum yield ranging from 0.0057 to 0.0080 molecules $photon^{-1}$. Indeed, a robust daily photolysis rate constant $\overline{J_{NO_3}}$ of $(3.94 \pm 0.68) \times 10^{-8}$ s^{-1} (1σ) was calculated for the Antarctic Plateau photic zone (0-50 cm layer). Daily summer NO_x fluxes at Dome C were estimated to be $(7.9 \pm 4.3) \times 10^{7}$ molec cm^{-2} s^{-1}, ~ 5 to 40 times less than what has been estimated in previous studies. Additionally, a preliminary 1-D model case-study confirmed our methodology and the coherence of the NO_x fluxes estimates using FC experiments. Such approach also reduced the estimate's uncertainties by a factor up to 20. By extrapolating our FC observations, a rough annual snow source NO_x budget of 0.045 ± 0.015 Tg.N y^{-1} was found for Antarctica, more than five times the estimated N-budget of the stratosphere denitrification source. Another source, such as long-range transport in the troposphere is necessary to explain the loss. Observations here are in agreement with Bock et al. (2016) and Chan et al. (2018) theories suggesting that a single dominant incorporation mechanism is controlling the nitrate deposition in snow (i.e., co-condensation) and that a young snow will locate the nitrate in the same place in the snow's ice crystal as an older snow at cold sites such as Dome C *(Bock et al., 2016; Chan et al., 2018)*. The large discrepancies previously observed on the F_{NO_x} estimates are attributable to the uncertainty of the transport component, for which the FC in our approach is insensitive. This is a strong argument that flux chambers are superior tools to measure NO_x flux as they are insensitive to the transport part. Their use should be increasingly used across the cryosphere to improve calculations of NO_x budgets as it appears that the snowpack photolytic source is rather significant for Antarctica as a whole and is potentially the dominant denitrification factor of the Antarctic cryosphere. Additionally, we found that the nitrate loss attributed to the mass loss of the Antarctic continent is roughly equivalent to the nitrate stratospheric input. This observation allows us to suggest that the nitrate budget in Antarctica is closed by considering that all NO_x produced by the snowpack denitrification are re-oxidized, making the balance null. As additional experiments using the methodology and equipment detailed here can also better constrain the nitrate photolysis description and the NO_x flux estimation, such experiments make it possible to refine parameters used to estimate NO_x production. Their results could help improve models by overcoming uncertainties on parameters traditionally used in models. With this technique, the NO_x snow source could be better defined and differences in photolytic mechanics between East and West Antarctica, Coast and Plateau, could be addressed. Knowledge gained in Antarctica may have broader impacts as well, as the re-emission of NO_x (re-noxification) of the atmosphere is a global phenomenon not limited to polar *(McCalley and Sparks, 2009; Michoud et al., 2015; Su et al., 2011)*.

Appendix 1 – Leighton equilibrium

Estimations of ozone concentration were calculated following Leighton's photostationary equilibrium *(Leighton, 1961)*:

$NO_2 + h\nu\ (\lambda < 420\ nm) \rightarrow NO + O\ (^3P)$ (RA.1)

$O\ (^3P) + O_2 + M \rightarrow O_3 + M$ (RA.2)

$NO + O_3 \rightarrow NO_2 + O_2$ (RA.3)

If equilibrium is reached, then the concentrations of the species involved can be derived following Equation (A1):

$$[O_3] = \frac{J_{NO_2}[NO_2]}{k_{NO}[NO]} \quad \text{(A1)}$$

where J_{NO_2} is the photolysis constant rate of reaction (RA.1) and k_{NO} is the reaction rate of reaction (R3). From Atkinson et al. (NIST Kinetics Database), the rate expression of k_{NO} is given by 1.4 x 10^{-12} exp (-10.89 [±1.66]/*RT*) expressed in cm^3 $molecules^{-1}$ s^{-1} and J_{NO_2} is taken from *(Kukui et al., 2014)*. [O_3] estimations were calculated at the daily maximum and in the meteorological conditions of the experiments. The O_3 levels expected from the Leighton relationship were > 100 ppbv where 0.7 to 10 ppbv where measured, confirming that equilibrium was not reached during the FC experiments.

Appendix 2 – Denitrification

Assuming one photolyzed molecule of NO_3^- produces one molecule of NO_x (Reactions R1 to R3 in the manuscript), the denitrification occurring during the experiments can be calculated following Equation (A2):

$$\%_{den} = 100x\frac{N_{NO_{x-total}}}{N_{NO_{3-total}^-}} \quad \text{(A2)}$$

With $N_{NO_{x-total}}$ the total number of molecules of NO_x emitted during one experiment and $N_{NO_{3-total}}$, the total number of NO_3^- molecules initially present in the chamber. $N_{NO_{3-total}}$ and $N_{NO_{x-total}}$ are calculated for each experiment following Equations (A3) and (A4):

$$N_{NO_{3-total}^-} = \rho_{snow}(g.cm^{-3})\frac{Na(molec.mol^{-1})}{MM_{NO_3^-}(g.mol^{-1})}[NO_3^-](g.g^{-1})V_{FC}(cm^3) \quad \text{(A3)}$$

$$N_{NO_{x-total}} = \rho_{air}(g.cm^{-3})\frac{Na(molec.mol^{-1})}{MM_{NO_x}(g.mol^{-1})}[NO_x](mol.mol^{-1})V_{FC}(cm^3) \quad \text{(A4)}$$

- N_A = Avogadro's number = 6.022 x 10^{23} molec mol^{-1}
- $M_{NO_3^-}$ = Molar mass of NO_3^- = 62.0049 g mol^{-1}
- M_{NO_x} = Molar mass of NO_x = 76.0155 g mol^{-1}
- V_{FC} = chamber volume ~ 26,500 cm^3
- ρ_{snow} = snow density calculated by gravimetry

- ρ_{air} = air density in the snow ~ 0.929 x10^{-3} g cm^{-3} at Dome C

Appendix 3 – NO_x emissions Fit

To estimate the NO_x concentration during the steady-state regime, we modeled the best fit of the [NO_x] emissions following Equation 5 in the manuscript and used the best fit estimates in analyses to refine the original measurement scattering.

Experiment	a	b	ω	ϕ
Local 40-50 cm	0.130	-0.118	7.968	-0.768
Local 10-20 cm	0.101	0.113	7.660	2.534
Local 2-7 cm	0.104	0.148	-7.100	3.923
Pristine* 30-40 cm	0.071	-0.077	7.775	-0.643
Pristine* 10-20 cm	0.119	-0.134	7.125	-0.461
Pristine* 2-7 cm	0.162	0.279	-7.443	3.833
Drift snow	1.958	1.683	7.674	-3.877

* Pristine snow correspond to the 25 km South of Concordia station samples

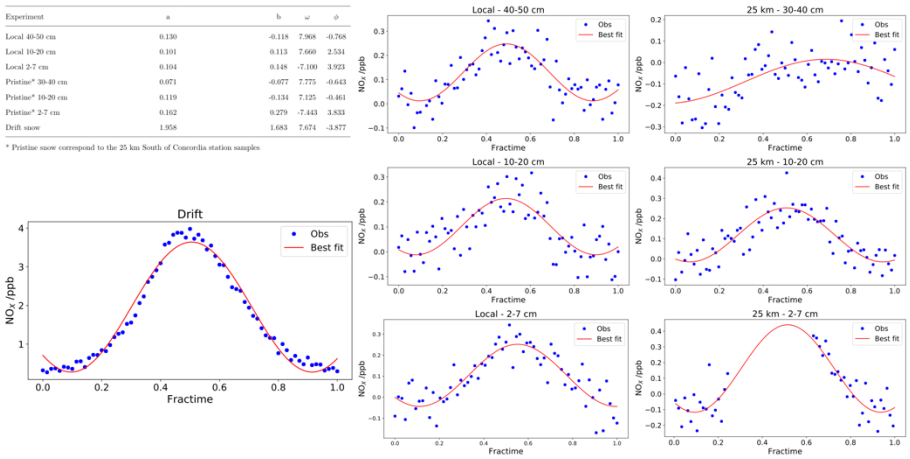

Figure A.3: (top left) *Table with the best fit parameters found for each experiment and the associated plots. Note that for the 2-7 cm 25 km experiment almost half a day of data were missing.*

Therefore, the total NO_x emissions over one day is calculated by the following Equation (A5):

$$\int_0^t [NO_x]dt = \int_0^t [a + b\cos(\omega t + \phi)]dt = [a + b\frac{\sin(\omega t + \phi)}{\omega} + cst]_0^t \quad \text{(A5)}$$

Appendix 4 – Nitrate snow content profile

As mentioned in the manuscript, snow pits have been sampled at Dome C for several years through the programs NITEDC and CAPOXI. All the data corresponding to the observation period of the FC experiments were averaged giving the following profile, Figure A.4:

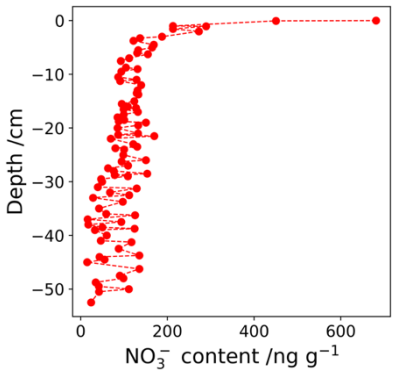

Figure A.4: *Profile of average NO_3^- concentration (ng g^{-1}) in the near surface snow column at Dome C.*

The average concentration of the photic zone is defined by the area under the averaged curve divided by the depth (Δz = 50cm), Equation (A6) hereafter, with z = -50cm:

$$[NO_3^-]_{mean} = \frac{\int_z^0 [NO_3^-]dz}{\Delta z} \quad \text{(A6)}$$

Using the trapezoidal rule, the average concentration found was $[NO_3^-] = 108 \pm 8$ ng g^{-1}.

Appendix 5 – Length of days at Dome C

Daylength calculation was made using a Center for Biosystems Modelling (CBM) model *(Forsythe et al., 1995)*. The model estimates daylength with error less than one minute within 40 degrees of the equator and less than seven minutes within 60 degrees, described by Equations (A7), (A8) and (A9):

$$\theta = 0.2163108 + 2\arctan(0.9671396\tan(0.00860(J - 186))) \quad \text{(A7)}$$

$$\phi = \arcsin(0.39795\cos(\theta)) \quad \text{(A8)}$$

$$D = 24 - \frac{24}{\pi}\arccos\left[\frac{\sin(\frac{p\pi}{180}) + \sin(\frac{L\pi}{180})\sin(\phi)}{\cos(\frac{L\pi}{180})\cos(\theta)}\right] \quad \text{(A9)}$$

With θ, the predicted revolution angle from the day of the year (J); ϕ the predicted sun's declination angle; D the predicted daylength from Latitude L, here L = -75.06. The daylength definition, defined by the position of the sun with respect to the horizon, chosen for this calculation is: sunrise/sunset is when the top of the sun is apparently even with horizon, giving p = 0.8333. Figure SI A.5 represents the length of day for one year at Dome C.

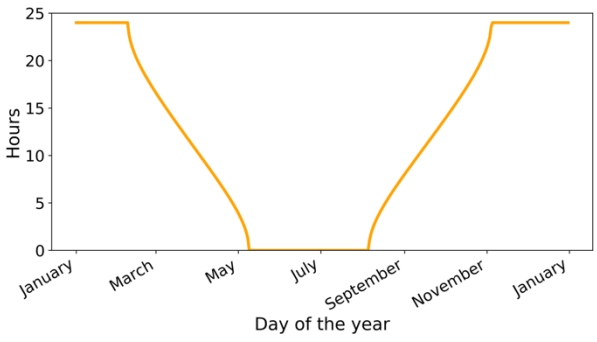

Figure A.5: *Hours of daylight over the year at Dome C.*

Appendix 6 – Boundary layer height from MAR at Dome C

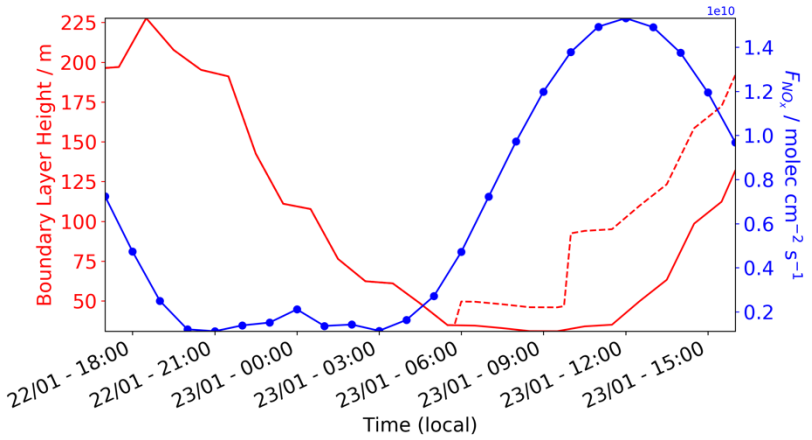

Figure A.6: *Boundary layer height from MAR at Dome C (red) and adjusted boundary layer height (dashed red) used in the PBLH run between the 22nd - 23rd of January 2020. NO_x flux ($F_{NO_x-hourly}$) calculated using the FC experiments between the 22nd - 23rd of January 2020 (blue).*

Acknowledgments

The research leading to these results has received funding from: the LabEx OSUG@2020 ("Investissements d'avenir" – ANR10 LABX56); the French National program LEFE (Les Enveloppes Fluides et l'Environnement) via LEFE REACT; the Agence Nationale de la Recherche (ANR) via contract ANR-16-CE01-0011-01 EAIIST; the Foundation BNP-Paribas through its Climate & Biodiversity Initiative program and by the French Polar Institute (IPEV) through programs 1177 (CAPOXI 35–75) and 1169 (EAIIST). The meteorological data and information were obtained from IPEV/PNRA Project "Routin Meteorological Observation at Station Concordia" http://www.climantartide.it. The data used in this publication for the irradiations fluxes were obtained from LATMOS, with the help of Florence Goutail et Jean-Pierre Pommereau as part of the Network for the Detection of Atmospheric Composition Change (NDACC) and are publicly available (see http://www.ndacc.org). The authors greatly thank Maria Zatko and Becky Alexander for the inputs on the global atmospheric chemistry modelling. We would like to thank Pete Akers for his help with reviewing the English of the manuscript. Finally, the authors greatly thank the technical staff of the IGE and IPEV for their technical support in Grenoble and during the field campaign.

Data availability. The data are available upon request.

Supplement. The supplement related to this article is available on-line at:

Author contributions. Grants obtained by JS and RG funded the project. The IBBCEAS instruments were designed and developed by CB under the supervision of RG. AB developed and validated the ozone generation. The instruments were optimized and validated by CB and AB, who also did the field installation

and observations. RG was the principal supervisor of the instrument development. Based on the original idea of JS, AB and JS developed the FC design under JS supervision and AB realized the validation tests. JS and RG are the supervisors of AB's PhD thesis under which the experiments are deployed. NC provided technical and engineering input particularly on the field. CA provided the MAR simulations to drive the 1-D model. SA provided the 1-D model simulation under the supervision of JT. GP provided the TARTE and SBDART scripts. JS, GP, MF, YH, CA, JT and RG contributed with their knowledge in atmospheric sciences and modeling. The paper was written by AB, with contributions from all authors. Section 4.4 was written by SA and JT and completed by CA.

Competing interests. The authors declare that they have no conflict of interest.

References

Agosta, C., Amory, C., Kittel, C., Orsi, A., Favier, V., Gallée, H., van den Broeke, M. R., Lenaerts, J. T. M., van Wessem, J. M., van de Berg, W. J. and Fettweis, X.: Estimation of the Antarctic surface mass balance using the regional climate model MAR (1979–2015) and identification of dominant processes, The Cryosphere, 13(1), 281–296, https://doi.org/10.5194/tc-13-281-2019, 2019.

Amory, C., Kittel, C., Le Toumelin, L., Agosta, C., Delhasse, A., Favier, V. and Fettweis, X.: Performance of MAR (v3.11) in simulating the drifting-snow climateand surface mass balance of Adelie Land, East Antarctica, preprint, Cryosphere., 2020.

Barbero, A., Blouzon, C., Savarino, J., Caillon, N., Dommergue, A. and Grilli, R.: A compact incoherent broadband cavity-enhanced absorption spectrometer for trace detection of nitrogen oxides, iodine oxide and glyoxal at levels below parts per billion for field applications, Atmos. Meas. Tech., 13(8), 4317–4331, https://doi.org/10.5194/amt-13-4317-2020, 2020.

Bauguitte, S. J.-B., Bloss, W. J., Evans, M. J., Salmon, R. A., Anderson, P. S., Jones, A. E., Lee, J. D., Saiz-Lopez, A., Roscoe, H. K., Wolff, E. W. and Plane, J. M. C.: Summertime NOx measurements during the CHABLIS campaign: can source and sink estimates unravel observed diurnal cycles?, Atmos. Chem. Phys., 12(2), 989–1002, https://doi.org/10.5194/acp-12-989-2012, 2012.

Becagli, S., Proposito, M., Benassai, S., Flora, O., Genoni, L., Gragnani, R., Largiuni, O., Pili, S. L., Severi, M., Stenni, B., Traversi, R., Udisti, R. and Frezzotti, M.: Chemical and isotopic snow variability in East Antarctica along the 2001/02 ITASE traverse, Ann. Glaciol., 39, 473–482, https://doi.org/10.3189/172756404781814636, 2004.

Beine, H. J., Honrath, R. E., Dominé, F., Simpson, W. R. and Fuentes, J. D.: NOx during background and ozone depletion periods at Alert: Fluxes above the snow surface, Journal of Geophysical Research, 107(D21), 12, https://doi.org/10.1029/2002JD002082, 2002.

Besnard, K. and Pokryszka, Z.: Gases emission monitoring in a post-mining context, Symposium Post Mining 2005, Nancy, France, ineris–00972521, 12, 2005.

Blaszczak-Boxe, C. S. and Saiz-Lopez, A.: Nitrate photolysis in ice and snow: A critical review of its multiphase chemistry, Atmospheric Environment, 193, 224–241, https://doi.org/10.1016/j.atmosenv.2018.09.002, 2018.

Bloss, W. J., Evans, M. J., Lee, J. D., Sommariva, R., Heard, D. E. and Pilling, M. J.: The oxidative capacity of the troposphere: Coupling of field measurements of OH and a global chemistry transport model, Faraday Discuss., 130, 425, https://doi.org/10.1039/b419090d, 2005.

Bock, J., Savarino, J. and Picard, G.: Air–snow exchange of nitrate: a modelling approach to investigate physicochemical processes in surface snow at Dome C, Antarctica, Atmos. Chem. Phys., 16(19), 12531–12550, https://doi.org/10.5194/acp-16-12531-2016, 2016.

Brandt, R. E. and Warren, S. G.: Solar-heating rates and temperature profiles in Antarctic snow and ice, Journal of Glaciology, 39, 12, https://doi.org/10.3189/s0022143000015756, 1993.

Browne, E. C., Wooldridge, P. J., Min, K.-E. and Cohen, R. C.: On the role of monoterpene chemistry in the remote continental boundary layer, Atmos. Chem. Phys., 14(3), 1225–1238, https://doi.org/10.5194/acp-14-1225-2014, 2014.

Burkholder, J., Talukdar, A., Ravishankar, A. R. and Susansolomon, A.: Temperature Dependence of the HNO3 UV Absorption Cross, Journal of Geophysical Research, 98, 22,937-22,948, https://doi-org.gaelnomade-2.grenet.fr/10.1029/93JD02178, 1993.

Burley, J. D. and Johnston, H. S.: Ionic mechanisms for heterogeneous stratospheric reactions and ultraviolet photoabsorption cross sections for NO2, HNO3, and NO3 in sulfuric acid, Geophysical Research Letters, 19(13), 1359–1362,

https://doi.org/10.1029/92GL01115, 1992.

Cao, L., Platt, U. and Gutheil, E.: Role of the boundary layer in the occurrence and termination of the tropospheric ozone depletion events in polar spring, Atmospheric Environment, 132, 98–110, https://doi.org/10.1016/j.atmosenv.2016.02.034, 2016.

Chan, H. G., Frey, M. M. and King, M. D.: Modelling the physical multiphase interactions of HNO3 between snow and air on the Antarctic Plateau (Dome C) and coast (Halley), Atmos. Chem. Phys., 18(3), 1507–1534, https://doi.org/10.5194/acp-18-1507-2018, 2018.

Chu, L. and Anastasio, C.: Quantum Yields of hydroxyl radical and nitrogen dioxide from the photolysis of nitrate on ice, J. Phys. Chem. A, 107(45), 9594–9602, https://doi.org/10.1021/jp0349132, 2003.

Cotel, S., Schäfer, G., Traverse, S., Marzougui-Jaafar, S., Gay, G. and Razakarisoa, O.: Evaluation of VOC fluxes at the soil-air interface using different flux chambers and a quasi-analytical approach, Water Air Soil Pollut, 226(11), 356, https://doi.org/10.1007/s11270-015-2596-y, 2015.

Cotter, E. S. N., Jones, A. E. and Wolff, E. W.: What controls photochemical NO and NO2 production from Antarctic snow? Laboratory investigation assessing the wavelength and temperature dependence, Journal of Geophysical Research, 108(D4), 10, https://doi.org/10.1029/2002JD002602, 2003.

Davis, D., Seelig, J., Huey, G., Crawford, J., Chen, G., Wang, Y., Buhr, M., Helmig, D., Neff, W. and Blake, D.: A reassessment of Antarctic plateau reactive nitrogen based on ANTCI 2003 airborne and ground based measurements, Atmospheric Environment, 42(12), 2831–2848, https://doi.org/10.1016/j.atmosenv.2007.07.039, 2008.

Deshler, T., Adriani, A., Hofmann, D. J. and Gobbi, G. P.: Evidence for denitrification in the 1990 Antarctic spring stratosphere: II. Lidar and aerosol measurements, Geophys. Res. Lett., 18(11), 1999–2002, https://doi.org/10.1029/91GL02311, 1991.

Domine, F. and Shepson, P. B.: Air-Snow Interactions and Atmospheric Chemistry, Science, 297(5586), 1506–1510, https://doi.org/10.1126/science.1074610, 2002.

Domine, F. and Thibert, E.: Relationship between atmospheric composition and snow composition for HCl and HNO3, Biogeochemistry of Seasonally Snow-Covered Catchments, 228, 3–10, 1995.

Domine, F., Albert, M., Huthwelker, T. and Simpson, W. R.: Snow physics as relevant to snow photochemistry, Atmos. Chem. Phys., 8, 171–208, https://doi.org/10.5194/acp-8-171-2008, 2008.

Ehhalt, D., Prather, M., Dentener, F., Derwent, R., Dlugokencky, E., Holland, E., Isaksen, I., Katima, J., Kirchhoff, V., Matson, P., Midgley, P., Wang, M., Berntsen, T., Bey, I., Brasseur, G., Buja, L., Collins, W. J., Daniel, J., DeMore, W. B., Derek, N., Dickerson, R., Etheridge, D., Feichter, J., Fraser, P., Friedl, R., Fuglestvedt, J., Gauss, M., Grenfell, L., Grübler, A., Harris, N., Hauglustaine, D., Horowitz, L., Jackman, C., Jacob, D., Jaeglé, L., Jain, A., Kanakidou, M., Karlsdottir, S., Ko, M., Kurylo, M., Lawrence, M., Logan, J. A., Manning, M., Mauzerall, D., McConnell, J., Mickley, L., Montzka, S., Müller, J. F., Olivier, J., Pickering, K., Pitari, G., Roelofs, G. J., Rogers, H., Rognerud, B., Smith, S., Solomon, S., Staehelin, J., Steele, P., Stevenson, D., Sundet, J., Thompson, A., van Weele, M., Joos, F. and McFarland, M.: Atmospheric Chemistry and Greenhouse Gases, IPCC, 240–287, 2018.

Eklund, B.: Practical guidance for flux chamber measurements of fugitive volatile organic emission rates, Journal of the Air & Waste Management Association, 42(12), 1583–1591, https://doi.org/10.1080/10473289.1992.10467102, 1992.

Erbland, J., Vicars, W. C., Savarino, J., Morin, S., Frey, M. M., Frosini, D., Vince, E. and Martins, J. M. F.: Air–snow transfer of nitrate on the East Antarctic Plateau – Part 1: Isotopic evidence for a photolytically driven dynamic equilibrium in summer, Atmos. Chem. Phys., 13(13), 6403–6419, https://doi.org/10.5194/acp-13-6403-2013, 2013.

Erbland, J., Savarino, J., Morin, S., France, J. L., Frey, M. M. and King, M. D.: Air–snow transfer of nitrate on the East Antarctic Plateau – Part 2: An isotopic model for the interpretation of deep ice-core records, Atmospheric Chemistry and Physics, 15(20), 12079–12113, https://doi.org/10.5194/acp-15-12079-2015, 2015.

Fabre, A., Barnola, J.-M., Arnaud, L. and Chappellaz, J.: Determination of gas diffusivity in polar firn: comparison between experimental measurements and inverse modeling, Geophys. Res. Lett., 27(4), 557–560, https://doi.org/10.1029/1999GL010780, 2000.

Fahey, D. W., Kelly, K. K., Kawa, S. R., Tuck, A. F., Loewenstein, M., Chan, K. R. and Heidt, L. E.: Observations of denitrification and dehydration in the winter polar stratospheres, Nature, 344, 321–324, https://doi.org/10.1038/344321a0, 1990.

Finlayson-Pitts, B. J. and Pitts, J. N.: Spectroscopy and photochemistry - Fundamentals, in Chemistry of the Upper and Lower Atmosphere, edited by B. J. Finlayson-Pitts and J. N. Pitts, pp. 43–85, Academic Press, San Diego, https://doi.org/10.1016/B978-012257060-5/50006-X, , 2000.

Forsythe, W. C., Rykiel, E. J., Stahl, R. S., Wu, H. and Schoolfield, R. M.: A model comparison for daylength as a function of latitude and day of year, Ecological Modelling, 80(1), 87–95, https://doi.org/10.1016/0304-3800(94)00034-F, 1995.

France, J. L., King, M. D., Frey, M. M., Erbland, J., Picard, G., Preunkert, S., MacArthur, A. and Savarino, J.: Snow optical properties at Dome C (Concordia), Antarctica; implications for snow emissions and snow chemistry of reactive nitrogen, Atmos. Chem. Phys., 11(18), 9787–9801, https://doi.org/10.5194/acp-11-9787-2011, 2011.

Frey, M. M., Savarino, J., Morin, S., Erbland, J. and Martins, J. M. F.: Photolysis imprint in the nitrate stable isotope signal in snow and atmosphere of East Antarctica and implications for reactive nitrogen cycling, Atmos. Chem. Phys., 9(22), 8681–8696, https://doi.org/10.5194/acp-9-8681-2009, 2009.

Frey, M. M., Brough, N., France, J. L., Anderson, P. S., Traulle, O., King, M. D., Jones, A. E., Wolff, E. W. and Savarino, J.: The diurnal variability of atmospheric nitrogen oxides (NO and NO2) above the Antarctic Plateau driven by atmospheric stability and snow emissions, Atmos. Chem. Phys., 13(6), 3045–3062, https://doi.org/10.5194/acp-13-3045-2013, 2013a.

Frey, M. M., Brough, N., France, J. L., Anderson, P. S., Traulle, O., King, M. D., Jones, A. E., Wolff, E. W. and Savarino, J.: The diurnal variability of atmospheric nitrogen oxides (NO and NO2) above the Antarctic plateau driven by atmospheric stability and snow emissions, Atmos. Chem. Phys., 13(6), 3045–3062, https://doi.org/10.5194/acp-13-3045-2013, 2013b.

Frey, M. M., Roscoe, H. K., Kukui, A., Savarino, J., France, J. L., King, M. D., Legrand, M. and Preunkert, S.: Atmospheric nitrogen oxides (NO and NO2) at Dome C, East Antarctica, during the OPALE campaign, Atmos. Chem. Phys., 15(14), 7859–7875, https://doi.org/10.5194/acp-15-7859-2015, 2015a.

Frey, M. M., Roscoe, H. K., Kukui, A., Savarino, J., France, J. L., King, M. D., Legrand, M. and Preunkert, S.: Atmospheric nitrogen oxides (NO and NO2) at Dome C, East Antarctica, during the OPALE campaign, Atmos. Chem. Phys., 15(14), 7859–7875, https://doi.org/10.5194/acp-15-7859-2015, 2015b.

Gallée, H. and Gorodetskaya, I. V.: Validation of a limited area model over Dome C, Antarctic Plateau, during winter, Clim Dyn, 34(1), 61–72, https://doi.org/10.1007/s00382-008-0499-y, 2010.

Gallée, H., Preunkert, S., Argentini, S., Frey, M. M., Genthon, C., Jourdain, B., Pietroni, I., Casasanta, G., Barral, H., Vignon, E., Amory, C. and Legrand, M.: Characterization of the boundary layer at Dome C (East Antarctica) during the OPALE summer campaign, Atmos. Chem. Phys., 15(11), 6225–6236, https://doi.org/10.5194/acp-15-6225-2015, 2015.

Gallet, J.-C., Domine, F., Arnaud, L., Picard, G. and Savarino, J.: Vertical profile of the specific surface area and density of the snow at Dome C and on a transect to Dumont D'Urville, Antarctica – albedo calculations and comparison to remote sensing products, The Cryosphere, 5(3), 631–649, https://doi.org/10.5194/tc-5-631-2011, 2011.

Grannas, A. M., Jones, A. E., Dibb, J., Ammann, M., Anastasio, C., Beine, H. J., Bergin, M., Bottenheim, J., Boxe, C. S., Carver, G., Chen, G., Crawford, J. H., Domine, F., Frey, M. M., Guzman, M. I., Heard, D. E., Helmig, D., Hoffmann, M. R., Honrath, R. E., Huey, L. G., Hutterli, M., Jacobi, H. W., Klan, P., Lefer, B., McConnell, J., Plane, J., Sander, R., Savarino, J., Shepson, P. B., Simpson, W. R., Sodeau, J. R., Weller, R., Wolff, E. W. and Zhu, T.: An overview of snow photochemistry: evidence, mechanisms and impacts, Atmos. Chem. Phys., 7, 4329–4373, https://doi.org/10.5194/acp-7-4329-2007, 2007.

Grilli, R., Legrand, M., Kukui, A., Méjean, G., Preunkert, S. and Romanini, D.: First investigations of IO, BrO, and NO2 summer atmospheric levels at a coastal East Antarctic site using mode-locked cavity enhanced absorption spectroscopy, Geophys. Res. Lett., 40(4), 791–796, https://doi.org/10.1002/grl.50154, 2013.

Helmig, D., Liptzin, D., Hueber, J. and Savarino, J.: Impact of exhaust emissions on chemical snowpack composition at Concordia Station, Antarctica, The Cryosphere, 14(1), 199–209, https://doi.org/10.5194/tc-14-199-2020, 2020.

Honrath, R. E., Peterson, M. C., Guo, S., Dibb, J. E., Shepson, P. B. and Campbell, B.: Evidence of NOx production within or upon ice particles in the Greenland snowpack, Geophys. Res. Lett., 26(6), 695–698, https://doi.org/10.1029/1999GL900077, 1999.

Honrath, R. E., Guo, S., Peterson, M. C., Dziobak, M. P., Dibb, J. E. and Arsenault, M. A.: Photochemical production of gas phase NOx from ice crystal NO3-, J. Geophys. Res., 105(D19), 24183–24190, https://doi.org/10.1029/2000JD900361, 2000.

Honrath, R. E., Lu, Y., Peterson, M. C., Dibb, J. E., Arsenault, M. A., Cullen, N. J. and Steffen, K.: Vertical fluxes of NOx, HONO, and HNO3 above the snowpack at Summit, Greenland, Atmospheric Environment, 36, 2629–2640, https://doi.org/10.1016/S1352-2310(02)00132-2, 2002.

Huang, Y., Wu, S., Kramer, L. J., Helmig, D. and Honrath, R. E.: Surface ozone and its precursors at Summit, Greenland: comparison between observations and model simulations, Atmos. Chem. Phys., 17(23), 14661–14674, https://doi.org/10.5194/acp-17-14661-2017, 2017.

Jones, A. E., Weller, R., Wolff, E. W. and Jacobi, H.-W.: Speciation and rate of photochemical NO and NO2 production in Antarctic snow, Geophys. Res. Lett., 27(3), 345–348, https://doi.org/10.1029/1999GL010885, 2000.

Jones, A. E., Weller, R., Anderson, P. S., Jacobi, H.-W., Wolff, E. W., Schrems, O. and Miller, H.: Measurements of NOx emissions from the Antarctic snowpack, Geophys. Res. Lett., 28(8), 1499–1502, https://doi.org/10.1029/2000GL011956, 2001.

Jones, A. E., Wolff, E. W., Ames, D., Bauguitte, S. J.-B., Clemitshaw, K. C., Fleming, Z., Mills, G. P., Saiz-Lopez, A., Salmon, R. A., Sturges, W. T. and Worton, D. R.: The multi-seasonal NOy budget in coastal Antarctica and its link with surface snow and ice core nitrate: results from the CHABLIS campaign, Atmos. Chem. Phys., 11(17), 9271–9285, https://doi.org/10.5194/acp-11-9271-2011, 2011.

Kenagy, H. S., Sparks, T. L., Ebben, C. J., Wooldrige, P. J., Lopez-Hilfiker, F. D., Lee, B. H., Thornton, J. A., McDuffie, E. E., Fibiger, D. L., Brown, S. S., Montzka, D. D., Weinheimer, A. J., Schroder, J. C., Campuzano-Jost, P., Day, D. A., Jimenez, J. L., Dibb, J. E., Campos, T., Shah, V., Jaeglé, L. and Cohen, R. C.: NO_x Lifetime and NO_y Partitioning During WINTER, J. Geophys. Res. Atmos., 123(17), 9813–9827, https://doi.org/10.1029/2018JD028736, 2018.

Kittel, C., Amory, C., Agosta, C., Jourdain, N. C., Hofer, S., Delhasse, A., Doutreloup, S., Huot, P.-V., Lang, C., Fichefet, T. and Fettweis, X.: Diverging future surface mass balance between the Antarctic ice shelves and grounded ice sheet, preprint, Ice sheets/Antarctic., 2020.

Kukui, A., Legrand, M., Preunkert, S., Frey, M. M., Loisil, R., Gil Roca, J., Jourdain, B., King, M. D., France, J. L. and Ancellet, G.: Measurements of OH and RO2 radicals at Dome C, East Antarctica, Atmos. Chem. Phys., 14(22), 12373–12392, https://doi.org/10.5194/acp-14-12373-2014, 2014.

Legrand, M., Preunkert, S., Frey, M., Bartels-Rausch, Th., Kukui, A., King, M. D., Savarino, J., Kerbrat, M. and Jourdain, B.: Large mixing ratios of atmospheric nitrous acid (HONO) at Concordia (East Antarctic Plateau) in summer: a strong source from surface snow?, Atmos. Chem. Phys., 14(18), 9963–9976, https://doi.org/10.5194/acp-14-9963-2014, 2014.

Leighton, P. A.: Photochemistry of Air Pollution, New York., 1961.

Lenschow, D. H.: Micrometeorological techniques for measuring biosphere-atmosphere trace gas exchange, P. A. Matson&R. C. Hariss., 1995.

Libois, Q., Picard, G., France, J. L., Arnaud, L., Dumont, M., Carmagnola, C. M. and King, M. D.: Influence of grain shape on light penetration in snow, The Cryosphere, 7, 1803–1818, https://doi.org/doi:10.5194/tc-7-1803-2013, 2013.

Libois, Q., Picard, G., Dumont, M., Arnaud, L., Sergent, C., Pougatch, E., Sudul, M. and Vial, D.: Experimental determination of the absorption enhancement parameter of snow, J. Glaciol., 60(222), 714–724, https://doi.org/10.3189/2014JoG14J015, 2014.

Madronich, S.: Photodissociation in the Atmosphere 1. Actinic Flux and the Effects of Ground Reflections and Clouds, Journal of Geophysical Research, 92(D8), 9740–975214, https://doi.org/10.1029/JD092iD08p09740, 1987.

Madronich, S. and Flocke, S.: The Role of Solar Radiation in Atmospheric Chemistry, in Environmental Photochemistry, vol. 2 / 2L, edited by P. Boule, pp. 1–26, Springer Berlin Heidelberg, Berlin, Heidelberg, https://doi.org/10.1007/978-3-540-69044-3_1, , 1999.

Masclin, S., Frey, M. M., Rogge, W. F. and Bales, R. C.: Atmospheric nitric oxide and ozone at the WAIS Divide deep coring site: a discussion of local sources and transport in West Antarctica, Atmos. Chem. Phys., 13(17), 8857–8877, https://doi.org/10.5194/acp-13-8857-2013, 2013.

Mauldin, R., Kosciuch, E., Eisele, F., Huey, G., Tanner, D., Sjostedt, S., Blake, D., Chen, G., Crawford, J. and Davis, D.: South Pole Antarctica observations and modeling results: new insights on HOx radical and sulfur chemistry, Atmospheric Environment, 44(4), 572–581, https://doi.org/10.1016/j.atmosenv.2009.07.058, 2010.

Mauldin, R. L., Eisele, F. L., Tanner, D. J., Kosciuch, E., Shetter, R., Lefer, B., Hall, S. R., Nowak, J. B., Buhr, M., Chen, G., Wang, P. and Davis, D.: Measurements of OH, H2SO4 and MSA at the South Pole during ISCAT, Geophys. Res. Lett., 28(19), 3629–3632, https://doi.org/10.1029/2000GL012711, 2001.

Mauldin, R. L., Kosciuch, E., Henry, B., Eisele, F. L., Shetter, R., Lefer, B., Chen, G., Davis, D., Huey, G. and Tanner, D.: Measurements of OH, HO2+RO2, H2SO4, and MSA at the South Pole during ISCAT 2000, Atmospheric Environment, 38(32), 5423–5437, https://doi.org/10.1016/j.atmosenv.2004.06.031, 2004.

McCalley, C. K. and Sparks, J. P.: Abiotic gas formation drives nitrogen loss from a desert ecosystem, Science, 326(5954), 837–840, https://doi.org/10.1126/science.1178984, 2009.

Meur, E. L., Magand, O., Arnaud, L., Fily, M., Frezzotti, M., Cavitte, M., Mulvaney, R. and Urbini, S.: Spatial and temporal distributions of surface mass balance between Concordia and Vostok stations, Antarctica, from combined radar and ice core data: first results and detailed error analysis, The Cryosphere, 20, https://doi.org/10.5194/tc-12-1831-2018, 2018.

Meusinger, C., Berhanu, T. A., Erbland, J., Savarino, J. and Johnson, M. S.: Laboratory study of nitrate photolysis in Antarctic snow. I. Observed quantum yield, domain of photolysis, and secondary chemistry, The Journal of Chemical Physics, 140(24), 244305, https://doi.org/10.1063/1.4882898, 2014.

Michoud, V., Doussin, J.-F., Colomb, A., Afif, C., Borbon, A., Camredon, M., Aumont, B., Legrand, M. and Beekmann, M.: Strong HONO formation in a suburban site during snowy days, Atmospheric Environment, 116, 155–158, https://doi.org/10.1016/j.atmosenv.2015.06.040, 2015.

Mulvaney, R. and Wolff, E. W.: Evidence for winter/spring denitrification of the stratosphere in the nitrate record of Antarctic firn cores, J. Geophys. Res., 98(D3), 5213–5220, https://doi.org/10.1029/92JD02966, 1993.

Noro, K. and Takenaka, N.: Post-depositional loss of nitrate and chloride in Antarctic snow by photolysis and sublimation: a field investigation, Polar Research, 39, 5146–5155, https://doi.org/10.33265/polar.v39.5146, 2020.

Oncley, S. P., Buhr, M., Lenschow, D. H., Davis, D. and Semmer, S. R.: Observations of summertime NO fluxes and boundary-layer height at the South Pole during ISCAT 2000 using scalar similarity, Atmospheric Environment, 38(32), 5389–5398, https://doi.org/10.1016/j.atmosenv.2004.05.053, 2004.

Palchetti, L., Bianchini, G., Di Natale, G. and Del Guasta, M.: Far-Infrared radiative properties of water vapor and clouds in antarctica, Bulletin of the American Meteorological Society, 96(9), 1505–1518, https://doi.org/10.1175/BAMS-D-13-00286.1, 2015.

Pinzer, B. R., Kerbrat, M., Huthwelker, T., Gaggeler, H. W., Schneebeli, M. and Ammann, M.: Diffusion of NOx and HONO in snow: a laboratory study, Journal of Geophysical Research, 115(D03304), 12, https://doi.org/doi:10.1029/2009JD012459, 2010, 2010.

Pokryszka, Z. and Tauziède, C.: Method of measuring surface emissions of methane, International Conference on Latest Achievements in the Field of Mine Ventilation Fire and Methane Hazrad Fighting, 277–283, 1999.

Preunkert, S., Ancellet, G., Legrand, M., Kukui, A., Kerbrat, M., Sarda-Estève, R., Gros, V. and Jourdain, B.: Oxidant Production over Antarctic Land and its Export (OPALE) project: an overview of the 2010-2011 summer campaign: overview of the OPALE project 2010-2011, J. Geophys. Res., 117(D15), 307–319, https://doi.org/10.1029/2011JD017145, 2012.

Rattigan, O., Lutman, E., Jones, R. L. and Coxt, R. A.: Temperature-dependent absorption cross-sections of gaseous nitric acid and methyl nitrate, Journal of Photochemistry and Photobiology A: Chemistry, 66, 313–326, https://doi.org/10.1002/bbpc.19920960331, 1992.

Ricchiazzi, P., Yang, S., Gautier, C. and Sowle, D.: SBDART: a research and teaching software tool for plane-parallel radiative transfer in the Earth's atmosphere, Bulletin of the American Meteorological Society, 79(10), 14, https://doi.org/10.1175/1520-0477(1998)079<2101:SARATS>2.0.CO;2, 1998.

Rignot, E., Mouginot, J., Scheuchl, B., van den Broeke, M., van Wessem, M. J. and Morlighem, M.: Four decades of Antarctic Ice Sheet mass balance from 1979–2017, Proc Natl Acad Sci USA, 116(4), 1095–1103, https://doi.org/10.1073/pnas.1812883116, 2019.

Saiz-Lopez, A., Borge, R., Notario, A., Adame, J. A., Paz, D. de la, Querol, X., Artíñano, B., Gómez-Moreno, F. J. and Cuevas, C. A.: Unexpected increase in the oxidation capacity of the urban atmosphere of Madrid, Spain, Sci Rep, 7(1), 45956, https://doi.org/10.1038/srep45956, 2017.

Salawitch, R. J., Gobbi, G. P., Wofsy, S. C. and McElroy, M. B.: Denitrification in the Antarctic stratosphere, Nature, 339, 525–527, https://doi.org/10.1038/339525a0, 1989.

Santee, M. L., Read, W. G., Waters, J. W., Froidevaux, L., Manney, G. L., Flower, D. A., Jarnot, R. F., Harwood, R. S. and Peckham, G. E.: Interhemispheric differences in polar stratospheric HNO3, H2O, ClO, and O3, Science, 267, 849–852, https://doi.org/10.1126/science.267.5199.849, 1995.

Savarino, J., Kaiser, J., Morin, S., Sigman, D. M. and Thiemens, M. H.: Nitrogen and oxygen isotopic constraints on the origin of atmospheric nitrate in coastal Antarctica, Atmos. Chem. Phys., 7, 1925–1945, https://doi.org/10.5194/acp-7-1925-2007, 2007.

Savarino, J., Vicars, W. C., Legrand, M., Preunkert, S., Jourdain, B., Frey, M. M., Kukui, A., Caillon, N. and Gil Roca, J.: Oxygen

isotope mass balance of atmospheric nitrate at Dome C, East Antarctica, during the OPALE campaign, Atmospheric Chemistry and Physics, 16(4), 2659–2673, https://doi.org/10.5194/acp-16-2659-2016, 2016.

Savitskiy, G. B. and Lessing, V. M.: Tropospheric jet streams in the Antarctic, Polar Geography, 3(3), 157–160, https://doi.org/10.1080/10889377909377113, 1979.

Scheutz, C., Bogner, J., Chanton, J. P., Blake, D., Morcet, M., Aran, C. and Kjeldsen, P.: Atmospheric emissions and attenuation of non-methane organic compounds in cover soils at a French landfill, Waste Management, 17, https://doi.org/10.1016/j.wasman.2007.09.010, 2008.

Shi, G., Buffen, A. M., Ma, H., Hu, Z., Sun, B., Li, C., Yu, J., Ma, T., An, C., Jiang, S., Li, Y. and Hastings, M. G.: Distinguishing summertime atmospheric production of nitrate across the East Antarctic Ice Sheet, Geochimica et Cosmochimica Acta, 231, 1–14, https://doi.org/10.1016/j.gca.2018.03.025, 2018.

Sihota, N. J., Singurindy, O. and Mayer, K. U.: CO2-Efflux Measurements for evaluating source zone natural attenuation rates in a petroleum hydrocarbon contaminated aquifer, Environmental Science & Technology, 45, 482–488, https://doi.org/10.1021/es1032585, 2010.

Simpson, W. R., King, M. D., Beine, H. J., Honrath, R. E. and Zhou, X.: Radiation-transfer modeling of snow-pack photochemical processes during ALERT 2000, Atmospheric Environment, 36(15–16), 2663–2670, https://doi.org/10.1016/S1352-2310(02)00124-3, 2002.

Sommerfeld, R. A., Knight, C. A. and Laird, S. K.: Diffusion of HNO3 in ice, Geophys. Res. Lett., 25(6), 935–938, https://doi.org/10.1029/98GL00413, 1998.

Stenni, B., Scarchilli, C., Masson-Delmotte, V., Schlosser, E., Ciardini, V., Dreossi, G., Grigioni, P., Bonazza, M., Cagnati, A., Karlicek, D., Risi, C., Udisti, R. and Valt, M.: Three-year monitoring of stable isotopes of precipitation at Concordia Station, East Antarctica, The Cryosphere, 10(5), 2415–2428, https://doi.org/10.5194/tc-10-2415-2016, 2016.

Su, H., Cheng, Y., Oswald, R., Behrendt, T., Trebs, I., Meixner, F. X., Andreae, M. O., Cheng, P., Zhang, Y. and Pöschl, U.: Soil nitrite as a source of atmospheric HONO and OH radicals, Science, 333, 1616–1618, https://doi.org/10.1126/science.1207687, 2011.

Thomas, J. L., Stutz, J., Lefer, B., Huey, L. G., Toyota, K., Dibb, J. E. and Glasow, R. V.: Modeling chemistry in and above snow at Summit, Greenland - Part 1: model description and results, Atmos. Chem. Phys., 11, 4899–4914, https://doi.org/doi:10.5194/acp-11-4899-2011, 2011.

Tillman, F. D., Choi, J.-W. and Smith, J. A.: A comparison of direct measurement and model simulation of total flux of volatile organic compounds from the subsurface to the atmosphere under natural field conditions: measurement and simulation of VOC flux, Water Resour. Res., 39(10), https://doi.org/10.1029/2003WR002098, 2003.

Traversi, R., Becagli, S., Brogioni, M., Caiazzo, L., Ciardini, V., Giardi, F., Legrand, M., Macelloni, G., Petkov, B., Preunkert, S., Scarchilli, C., Severi, M., Vitale, V. and Udisti, R.: Multi-year record of atmospheric and snow surface nitrate in the central Antarctic plateau, Chemosphere, 172, 341–354, https://doi.org/10.1016/j.chemosphere.2016.12.143, 2017.

Tuite, K., Thomas, J. L., Veres, P. R., Roberts, J. M., Stevens, P. S., Griffith, S. M., Dusanter, S., Flynn, J. H., Ahmed, S., Emmons, L., Kim, S.-W. and Stutz, J.: Quantifying nitrous acid formation mechanisms using measured vertical profiles during the CalNex 2010 campaign and 1D column modeling, J. Geophys. Res. Atmos., in review.

Valin, L. C., Russell, A. R. and Cohen, R. C.: Variations of OH radical in an urban plume inferred from NO2 column measurements: NO2 column and variations of OH radical, Geophys. Res. Lett., 40(9), 1856–1860, https://doi.org/10.1002/grl.50267, 2013.

Van Allen, R., Liu, X. and Murcray, F. J.: Seasonal variation of atmospheric nitric acid over the South Pole in 1992, Geophys. Res. Lett., 22(1), 49–52, https://doi.org/10.1029/94GL02794, 1995.

Verginelli, I., Pecoraro, R. and Baciocchi, R.: Using dynamic flux chambers to estimate the natural attenuation rates in the subsurface at petroleum contaminated sites, Science of The Total Environment, 619–620, 470–479, https://doi.org/10.1016/j.scitotenv.2017.11.100, 2018.

Volkamer, R., Sheehy, P., Molina, L. T. and Molina, M. J.: Oxidative capacity of the Mexico City atmosphere – Part 1: a radical source perspective, Atmos. Chem. Phys., 10, 6969–6991, https://doi.org/doi:10.5194/acp-10-6969-2010, 2010.

Wang, Y., Choi, Y., Zeng, T., Davis, D., Buhr, M., Gregory Huey, L. and Neff, W.: Assessing the photochemical impact of snow NOx emissions over Antarctica during ANTCI 2003, Atmospheric Environment, 41(19), 3944–3958, https://doi.org/10.1016/j.atmosenv.2007.01.056, 2007.

Werle, P., Mücke, R. and Slemr, F.: The limits of signal averaging in atmospheric trace-gas monitoring by tunable diode-laser absorption spectroscopy (TDLAS), Appl. Phys. B, 57(2), 131–139, https://doi.org/10.1007/BF00425997, 1993.

Winton, V. H. L., Ming, A., Caillon, N., Hauge, L., Jones, A. E., Savarino, J., Yang, X. and Frey, M. M.: Deposition, recycling, and archival of nitrate stable isotopes between the air–snow interface: comparison between Dronning Maud Land and Dome C, Antarctica, Atmos. Chem. Phys., 20(9), 5861–5885, https://doi.org/10.5194/acp-20-5861-2020, 2020.

Zatko, M., Geng, L., Alexander, B., Sofen, E. and Klein, K.: The impact of snow nitrate photolysis on boundary layer chemistry and the recycling and redistribution of reactive nitrogen across Antarctica and Greenland in a global chemical transport model, Atmos. Chem. Phys., 16(5), 2819–2842, https://doi.org/10.5194/acp-16-2819-2016, 2016.

Zatko, M. C., Grenfell, T. C., Alexander, B., Doherty, S. J., Thomas, J. L. and Yang, X.: The influence of snow grain size and impurities on the vertical profiles of actinic flux and associated NOx emissions on the Antarctic and Greenland ice sheets, Atmos. Chem. Phys., 13(7), 3547–3567, https://doi.org/10.5194/acp-13-3547-2013, 2013.

Zhu, C., Xiang, B., Zhu, L. and Cole, R.: Determination of absorption cross sections of surface-adsorbed HNO3 in the 290–330nm region by Brewster angle cavity ring-down spectroscopy, Chemical Physics Letters, 458(4–6), 373–377, https://doi.org/10.1016/j.cplett.2008.04.125, 2008.